UC Irvine
UC Irvine Previously Published Works

Title

Overexpression of glutamate–cysteine ligase protects human COV434 granulosa tumour cells against oxidative and γ-radiation-induced cell death

Permalink

https://escholarship.org/uc/item/0507k2xz

Journal

Mutagenesis, 24(3)

ISSN

0267-8357

Authors

Cortes-Wanstreet, Mabel M
Giedzinski, Erich
Limoli, Charles L
et al.

Publication Date

2009-05-01

DOI

10.1093/mutage/gen073

Peer reviewed

Overexpression of glutamate–cysteine ligase protects human COV434 granulosa tumour cells against oxidative and γ-radiation-induced cell death

Mabel M. Cortes-Wanstreet[1], Erich Giedzinski[2], Charles L. Limoli[2] and Ulrike Luderer[1,3,]*

[1]Department of Developmental and Cell Biology, [2]Department of Radiation Oncology and [3]Department of Medicine, University of California Irvine, Irvine, CA 92617, USA

Ionizing radiation is toxic to ovarian follicles and can cause infertility. Generation of reactive oxygen species (ROS) has been implicated in the toxicity of ionizing radiation in several cell types. We have shown that depletion of the antioxidant glutathione (GSH) sensitizes follicles and granulosa cells to toxicant-induced apoptosis and that supplementation of GSH is protective. The rate-limiting reaction in GSH biosynthesis is catalysed by glutamate–cysteine ligase (GCL), which consists of a catalytic subunit (GCLC) and a regulatory subunit (GCLM). We hypothesized that overexpression of *Gclc* or *Gclm* to increase GSH synthesis would protect granulosa cells against oxidant- and radiation-induced cell death. The COV434 line of human granulosa tumour cells was stably transfected with vectors designed for the constitutive expression of *Gclc*, *Gclm*, both *Gclc* and *Gclm* or empty vector. GCL protein and enzymatic activity and total GSH levels were significantly increased in the GCL subunit-transfected cells. GCL-transfected cells were resistant to cell killing by treatment with hydrogen peroxide compared to control cells. Cell viability declined less in all the GCL subunit-transfected cell lines 1–8 h after 0.5 mM hydrogen peroxide treatment than in control cells. We next examined the effects of GCL overexpression on responses to ionizing radiation. ROS were measured using a redox-sensitive fluorogenic dye in cells irradiated with 0, 1 or 5 Gy of γ-rays. There was a dose-dependent increase in ROS within 30 min in all cell lines, an effect that was significantly attenuated in *Gcl*-transfected cells. Apoptosis, assessed by terminal deoxynucleotidyl transferase-mediated deoxyuridine triphosphate nick-end labelling and activated caspase-3 immunoblotting, was significantly decreased in irradiated *Gclc*-transfected cells compared to irradiated control cells. Suppression of GSH synthesis in *Gclc*-transfected cells reversed resistance to radiation. These findings show that overexpression of GCL in granulosa cells can augment GSH synthesis and ameliorate various sequelae associated with exposure to oxidative stress and irradiation.

Introduction

Radiotherapy is based on the concept that exposure to sufficient doses of ionizing radiation will destroy target cells. Inherent to these treatments is the fact that non-target cells (i.e. normal tissue) will also be destroyed, and under certain clinical situations, damage to the limited pool of ovarian follicles may be unavoidable. Significant exposure to the ovaries occurs during radiotherapy of abdominal and pelvic cancers or when the pelvic lymph nodes are irradiated for haematological diseases such as Hodgkin's lymphoma (1). The ovaries also incur significant exposure when total body irradiation is used to treat various forms of leukaemia or when it is used to condition patients prior to bone marrow transplants (1). Together, chemotherapy and radiotherapy have dramatically increased the long-term survival of young cancer patients, but there are major side effects that can be directly linked to the damage of normal tissue surrounding the treatment area that adversely impact the quality of life of the patient (1,2). These include temporary cessation of ovarian function and premature ovarian failure (1,3–7).

It is generally accepted that mammalian females are born with a finite stock of ovarian follicles and that the survival and maturation of these follicles are essential for the preservation of fertility (1,8,9). Follicles consist of the oocyte surrounded by layers of somatic cells. The granulosa cell layers immediately surround the oocyte, and granulosa cells form direct intercellular connections with the oocyte. Surrounding the granulosa cells and separated from them by a basement membrane are the theca cells. Ovarian failure and permanent sterility are a direct result of complete follicular depletion, which occurs through the normal, age-associated processes of ovulation and follicular atresia and through exogenously induced follicular apoptosis. Atresia is a controlled apoptotic process of follicular degeneration (8–11). Ionizing radiation destroys the least mature primordial follicles as well as the maturing antral and secondary follicles (1–3,12). Destruction of maturing follicles appears to be driven by induction of apoptosis of the granulosa cells, which secondarily leads to death of the oocyte (11). Premature ovarian failure can occur as a result of the depletion of primordial follicle reserves by ionizing radiation (1–3,12). Temporary loss of fertility can occur when more mature follicles are destroyed, but some primordial follicles remain. The nearly complete destruction of primordial follicles in young adult mouse ovaries occurs 2 weeks after a single exposure to 0.1 Gy of ionizing radiation (13). Mathematical models have predicted that the estimated dose of abdominal, pelvic or total body irradiation required to destroy half of all the primordial follicles in young humans is <2 Gy (5,6). The extent of ovarian damage caused by radiotherapy is dependent upon three critical factors: the dose, the irradiation field and the patient's age, with older women having a greater risk of becoming infertile (1,2).

The molecular mechanisms underlying follicle destruction by radiation exposure are not completely understood. About one-third of DNA damage from irradiation is caused by direct ionizations to the DNA target molecule, while the remaining

two-thirds of the net DNA damage are due to the reactive species derived from the indirect ionization of water (14–16). The most reactive of these species is the hydroxyl radical, which generates clustered DNA damage when energy deposition events yielding several ion pairs are in close proximity to the DNA helix. Hydroxyl radicals and other reactive oxygen species (ROS) have the potential to damage critical cellular components. These include protein oxidation, lipid peroxidation and DNA damage including DNA–protein cross-linking and double-stranded DNA breaks (17–19). Despite the transience of radiation-induced free radicals, irradiation has been shown to elicit more persistent increases in oxidative stress. Increased ROS persisting hours, days and even weeks post-irradiation likely reflect perturbations to the redox homoeostasis of cells (20) and have been linked to functional changes at the mitochondrial level as well as other ROS generators such as the nicotinamide adenine dinucleotide phosphate (NADPH) oxidases (21). Radiation-induced oxidative stress can lead to elevated superoxide anion radical (SO) and hydrogen peroxide (H_2O_2), whose relatively longer half-lives permit more extensive diffusion throughout the cell, thereby amplifying the impact of past irradiation events (16). Therefore, scavenging free radicals through the use of radioprotectors (agents present during irradiation) and/or mitigators (agents present after irradiation) have the potential to reduce radiation- and metabolic-derived reactive species and provide a tractable strategy for attenuating radiation-induced cytotoxicity.

Glutathione (GSH) is the most abundant low-molecular weight, non-protein thiol in eukaryotic cells. It is maintained at millimolar concentrations in most cells (22,23). Despite its multiple and diverse functions, GSH is most often recognized as one of the cell's primary defences against exogenous xenobiotics and oxidative stress (22–24). GSH detoxifies ROS by spontaneous reduction, as in the case of hydroxyl radical, or by GSH peroxidase-mediated reduction, as in the case of H_2O_2 (22–24). GSH is synthesized by two sequential adenosine triphosphate (ATP)-dependent enzymatic reactions. The first and rate-limiting step is catalysed by glutamate–cysteine ligase (GCL), yielding γ-glutamylcysteine. The final step is catalysed by GSH synthetase and adds a glycine residue to yield γ-glutamylcysteinylglycine or GSH (22,23). GCL is a heterodimer composed of a catalytically active subunit (GCLC) that contains all substrate-binding sites and a regulatory subunit (GCLM) that modulates GCLC affinity for substrates and inhibitors (22,23,25).

Several previous studies provide support for the idea that GSH may be involved in radioprotection. Chemo- and radio-resistant cells have increased GSH levels (26–29). Depletion of GSH with the GCL-specific inhibitor L-buthionine sulfoximine (BSO) caused significant radiosensitization of A549 human lung cells (30,31). N-acetyl-cysteine (NAC), a GSH precursor, has been used as a radioprotective agent to attenuate acute liver injury, characterized by increased lipid peroxidation, GSH depletion, DNA single-strand breaks and hepatocyte apoptosis caused by X-rays in mice (32) and by total body γ-radiation in rats (33). These findings suggest that augmenting intracellular GSH levels can confer radiotolerance. Consequently, we set forth to genetically manipulate GSH concentrations of cells derived from a human granulosa cell tumour by overexpressing one or both subunits of GCL, the rate-limiting enzyme in GSH biosynthesis. We challenged these cells with various doses of pro-oxidants and γ-radiation to test the hypothesis that overexpression of GCL protects granulosa cells against oxidative and radiation-induced cell death.

Materials and methods

Chemicals

All chemicals were purchased from Sigma–Aldrich (St Louis, MO) or Fisher Scientific (Pittsburgh, PA), unless otherwise noted. Tissue culture reagents including all culture media, foetal bovine serum (FBS), 0.25% trypsin–ethylenediaminetetraacetic acid (EDTA), trypan blue, Lipofectamine 2000 Transfection Reagent and Geneticin (G418) were purchased from Invitrogen (Carlsbad, CA). All tissue culture vessels were obtained from Corning Costar (Lowell, MA).

COV434 cell line

The COV434 line of immortalized granulosa cells was derived from a primary human granulosa cell tumour and was kindly provided by Dr Peter I. Schrier (Department of Clinical Oncology, University Hospital, Leiden, The Netherlands) (34). The COV434 cells are diploid and, like normal granulosa cells, grow in small follicle-like aggregates, form intercellular junctions with neighbouring cells, form intercellular gap junctions with native cumulus cells when co-cultured with a cumulus–oocyte complex and increase cyclic adenosine 3′,5′-monophosphate and 17β-oestradiol in response to follicle-stimulating hormone and androstenedione co-stimulation (34–36).

COV434 cell culture

COV434 cells were maintained in Dulbecco's modified Eagle's medium–F12 (DMEM–F12) with GlutaMAX™ supplemented with 9% FBS, henceforth referred to as complete media, at 37°C in a humidified atmosphere of 95% air and 5% CO_2. Cells from passages 41–77 were used for the experiments reported herein. Cells were routinely harvested by trypsinization with 0.25% trypsin–EDTA, counted using a haemacytometer and 0.4% trypan blue and plated in complete media or complete media supplemented with 1 mg/ml G418. The doubling time of these cells is ∼24 h. Doubling times of the stably transfected cell lines were also ∼24 h.

Construction of Gclc and Gclm mammalian expression vectors

A full-length mouse *Gclc* cDNA cloned in the vector pCR2.1 (GCLc-pCR2.1) was a gift of Dr Julie K. Andersen (Buck Institute for Age Research, Novato, CA) (37). The *Gclc* cDNA was excised out of GCLc-pCR2.1 with the restriction endonucleases, BamHI and SalI, following the manufacturer's recommendations (New England BioLabs, Ipswich, MA). The pCMV-Script vector (Stratagene, La Jolla, CA) was cleaved using the same restriction endonucleases. Digested DNA fragments were isolated using the QIAquick PCR Purification Kit (Qiagen, Valencia, CA); purified fragments were electrophoresed through 2% agarose gels and isolated using the DNA Gel Extraction Kit as per the manufacturer's recommendations (Millipore, Billerica, MA). Cleaved vector was treated with calf intestinal alkaline phosphatase (New England BioLabs). *Gclc* cDNA was directionally subcloned downstream of the cytomegalovirus (CMV) promoter in the pCMV-Script vector using T4 DNA ligase (New England BioLabs). The resulting recombinant vectors, pCMVGCLC, were propagated in One Shot MAX Efficiency DH5α-T1® competent cells (Invitrogen) and plasmid preparations were performed using the QIAfilter Midi Plasmid Kit (Qiagen).

Dr Terrance J. Kavanagh (University of Washington, Seattle, WA) kindly provided us with a full-length mouse *Gclm* cDNA directionally cloned in pCR3.1-Uni, also a pCMV-directed mammalian expression vector that allows for the selection of stably transfected mammalian cells in media containing G418 antibiotic. This vector, GCLM-pCR3.1-Uni, will henceforth be referred to as pCMVGCLM vector (38). The *Gclm*-containing recombinant vector was propagated in One Shot MAX Efficiency DH5α-T1® competent cells and plasmid preparations were performed using the QIAfilter Midi Plasmid Kit.

All purified plasmid preparations were subjected to analytical restriction digests to identify correctly subcloned constructs. Vectors displaying the correct restriction map were subjected to CMVGCLC transgene-specific or CMVGCLM transgene-specific polymerase chain reaction (PCR) and/or automated sequence analysis at the UCI DNA Core Facility (University of California, Irvine, CA). Briefly, purified pCMVGCLC-Script vectors were amplified using the primer 5′-AATTAACCCTCACTAAAGGG-3′, which anneals to the 5′-flanking region just upstream of the ligation site beginning at nucleotide −109,where nucleotide +1 is the first nucleotide of the *Gclc* cDNA, and the primer 5′-GTAATAC-GACTCACTATAGGGC-3′, which anneals to the 3′ untranslated region of *Gclc* ending at nucleotide +2331, yielding an amplified product that is exactly 2.44 kb and spans part of the CMVGCLC transgene construct and the entire *Gclc* cDNA sequence. DNA sequencing has

repeatedly revealed 100% homology between pCMVGCLC-Script vector sequence and published pCMV-Script and *Gclc* cDNA sequences (37,38).

Purified pCMVGCLM vectors were amplified using the primer 5′-TAATACGACTCACTATAGGG-3′, which anneals to the 5′-flanking region just upstream of the ligation site beginning at nucleotide −60,where nucleotide +1 is the first nucleotide of the *Gclm* cDNA, and the primer 5′-TAGAAGGCACAGTCGAGG-3′, which anneals to the 3′ untranslated region ending at nucleotide +1052, yielding an amplified product that is exactly 1.112 kb and spans part of the CMVGCLM transgene construct and the entire *Gclm* cDNA sequence. DNA sequencing has repeatedly revealed 99.8% homology between pCMVGCLM vector sequence and published *Gclm* cDNA sequences, including one alanine to proline substitution at amino acid 7 and one silent mutation at amino acid 33 (codon CGA to codon CGG, both encoding for the amino acid arginine). DNA sequencing was performed at least two separate times and in duplicate for each cell line described in this report.

Stable transfection of COV434 cells

Cells from passage 44, for *Gclc* and empty vector control transfections, and cells from passage 36, for *Gclm* transfections and *Gclc*/*Gclm* co-transfections, were trypsinized and counted using trypan blue exclusion. Cells were plated at a density of 1.4×10^6 per well of a six-well tissue culture plate and were incubated for 24 h prior to transfection.

Four micrograms of plasmid DNA (pCMVGCLC-Script, pCMVGCLM, a 1:1 molar ratio of pCMVGCLC-Script to pCMVGCLM or empty pCMV-Script vectors) was diluted in 250 µl Opti-MEM I reduced serum medium. To form DNA–liposome complexes, 260 µl diluted Lipofectamine 2000 reagent was added to each diluted vector preparation and incubated for 20 min at room temperature. DNA–liposome complexes were added to each well containing COV434 cells, and cells were incubated for 6 h at 37°C. Transfection media were then replaced with complete media, and cells were incubated for 42 h. Cells were trypsinized and subcultured at 1:12 in 10-cm tissue culture plates using complete media freshly supplemented with 1 mg/ml G418 and ensuring that adherent cells covered no more than 50% of the growth surface area. Cells were grown for 10–14 days, feeding them selective complete media every 4 days.

Once there were visible colonies growing in the selective tissue culture plates, stably transfected cells were harvested using trypsinization within cloning cylinders adhered around a single colony using sterile vacuum grease. Cells from a single colony were transferred to a 24-well tissue culture plate in freshly prepared selective complete media. Cultures were grown to 80% confluency. Confluent cells were subcultured in progressively larger tissue culture vessels for a minimum of five passages prior to beginning experiments.

PCR to genotype stably transfected cells

Confluent cells were harvested by trypsinization and counted using trypan blue exclusion. In total, 4×10^6 cells were collected and pelleted by centrifugation at low speeds. Cells were washed with phosphate-buffered saline (PBS) and resuspended in PBS. Genomic DNA was extracted using the DNeasy Blood and Tissue Kit as per the manufacturer's instructions (Qiagen). One microgram genomic DNA was amplified using the CMVGCLC- or CMVGCLM-PCR using the primers described above.

For the CMVGCLC-PCR, DNA was denatured for 30 sec at 94°C, primers were annealed for 30 sec at 50°C and new DNA was polymerized for 2 min at 72°C for 32 cycles, yielding a 2.44-kb amplified product. For the CMVGCLM touchdown PCR, DNA was denatured for 30 sec at 94°C, primers were annealed for 30 sec at 65°C and new DNA was polymerized for 1 min at 72°C for 36 cycles. The annealing temperature was decreased in increments of 1°C in each subsequent set of cycles until 45°C was reached (cycle 21) at which time all annealing temperatures were held constant. This PCR yielded an amplified product that was exactly 1.112 kb. The genotyping of all the cell lines described in this report was performed at least three separate times throughout the course of these experiments.

GSH assay

Total intracellular GSH levels were measured using a modified form of an enzymatic recycling assay developed by Griffith (39,40). Cells were plated at 2×10^6 per 25-cm^2 flask using selective complete media and allowed to grow for 48 h. Cells were harvested by trypsinization and centrifuged at $300 \times g$ for 10 min. Cell pellets were lysed in ice-cold TES-SB buffer (20 mM Tris, 1 mM EDTA, 250 mM sucrose, 2 mM L-serine, 20 mM boric acid, supplemented with protease inhibitors, 100 µg/ml Pefabloc, 10 µg/ml n-alpha-p-tosyl-L-lysine chloromethyl ketone, 1 µg/ml pepstatin A, 1 µg/ml aprotinin and 1 µg/ml leupeptin) at a ratio of 50 µl buffer for every 2×10^6 cells. A small volume of cell homogenate was removed for subsequent protein assay with the Pierce bicinchoninic acid (BCA) Assay Kit (Pierce, Rockford, IL), and proteins were precipitated by acidifying the remaining cell homogenate with four parts homogenate to one part 5% sulfosalicylic acid (SSA). Homogenates were centrifuged at $15\,800 \times g$ for 10 min at 4°C. Sample aliquots were frozen at −80°C until use.

Standards containing known concentrations of GSH in TES-SB buffer with SSA or unknown samples were aliquoted in triplicate into the wells of a 96-well microplate, diluted with water and incubated at 30°C for 10 min. GSH reaction mixture [0.26 mM reduced β-NADPH, 0.74 mM 5,5-dithiobis(2-nitrobenzoic acid) (DTNB), 0.62 U/ml GSH reductase, 143 mM Na$_2$HPO$_4$ and 6.3 mM EDTA] was then added to each well. Absorbance was immediately monitored at 412 nm every 10 sec for 3.5 min using a VersaMax Tunable Microplate Reader with SOFTmax Pro version 3.1 Software (Molecular Devices, Sunnyvale, CA). DTNB is reduced to the yellow product 5-thio-2-nitrobenzoic acid with GSH acting as an electron donor. Oxidized glutathione is cycled back to its reduced form by GSH reductase and NADPH. The resulting slope of the absorbance versus time plot is proportional to the GSH concentration. The threshold of sensitivity for this assay is 0.04 nmol in our hands. Samples were analysed from four separate experiments.

Immunoblotting

Cells were plated at 2×10^6 per 25-cm^2 flask in selective complete media and allowed to grow for 24 or 48 h. Cells were then processed as for GSH assays, except the acidification step was omitted. Forty micrograms of protein samples were diluted in sample buffer containing sodium dodecyl sulphate and β-mercaptoethanol. Proteins were electrophoresed through 12% Tris–HCl polyacrylamide gels (Bio-Rad Laboratories, Hercules, CA) and then transferred to Immobilon-P transfer membranes (Millipore).

Protein blots from three separate experiments were probed and exposed to film simultaneously for GCLC and GCLM immunodetection. For activated caspase 3 immunodetection, cells from two separate experiments were analysed simultaneously. Blots were blocked at 4°C overnight using 5% non-fat dry milk in PBS supplemented with 0.1% Tween (PBST). Blots were then washed and incubated for 2 h at room temperature with a mixture of 1:40 000 rabbit anti-human GCLC and 1:20 000 rabbit anti-human GCLM (kind gift of Dr Terrance J. Kavanagh, University of Washington) (41) diluted in blocking solution of 3% non-fat dry milk, 3% bovine serum albumin (BSA), 1% ovalbumin, 1% normal goat serum and 0.1% sodium azide in PBST. Activated caspase 3 antibody (Asp 175, Cell Signaling, Beverly, MA) was used at a dilution of 1:100 in the same blocking solution. Blots were then washed and incubated for 1 h at room temperature with 1:10 000 horseradish peroxidase-conjugated donkey anti-rabbit IgG (Amersham Biosciences, Piscataway, NJ). The blots were washed and chemiluminescent detection was performed using the ECL Detection Kit and ECL Hyperfilm (both from Amersham Biosciences). Films were subjected to densitometric analyses to ascertain relative band intensities. The same blots were then probed for β-actin using 1:160 000 mouse anti-human β-actin (Sigma–Aldrich), followed by 1:10 000 horseradish peroxidase-conjugated anti-mouse IgG (Amersham Biosciences). GCLC and GCLM intensities were normalized to β-actin band intensities for the same sample, and results were expressed as fold the normalized CMV9b control levels for the same blot.

GCL enzymatic activity assay

GCL enzymatic activity was measured as first described by White *et al.* (42). Cells were plated at 2×10^6 per 25-cm^2 flask, cultured for 48 h and harvested and processed as for immunoblotting. Fifty microlitres of sample (in duplicate) or GSH standards in TES-SB were added in 20-sec intervals to prewarmed microcentrifuge tubes containing 50 µl of GCL reaction cocktail (400 mM Tris base, 40 mM ATP, 20 mM L-glutamic acid, 2 mM EDTA, 20 mM boric acid, 2 mM L-serine and 40 mM magnesium chloride hexahydrate). The GCL reaction was initiated by adding 50 µl of 2 mM L-cysteine to one of each of the sample tubes (GCL tube). After incubating for 20 min at 37°C, the GCL reaction was stopped by adding 50 µl of 200 mM SSA to all tubes. Immediately after the addition of SSA, 50 µl of 2 mM L-cysteine was added to the second tube of each sample (the baseline GSH tube) and to the GSH standard tubes. After the 20-min incubation on ice, all tubes were centrifuged for 5 min at $2000 \times g$ at 4°C. Twenty microlitres of supernatant was aliquoted in triplicate into the wells of a 96-well flat-bottomed, black-sided microplate. One hundred and eighty microlitres of 1.1 mM 2,3-naphthalenedicarboxaldehyde solution was then added to each well. The plate was incubated at room temperature for 30 min and read at an excitation wavelength of 485 nm and an emission wavelength of 535 nm using a GENios Plus Multi-Detection Microplate Reader with Enhanced Fluorescence (Tecan Group, Zurich, Switzerland). Results were expressed as the nanomoles of GSH synthesized above the baseline GSH level per minute per milligram protein, as determined using the Pierce BCA Protein Assay. There were three separate experiments performed for a total number of at least four samples per cell genotype.

Gamma irradiation of cells

Cells were irradiated in a J. L. Shepherd and Associates Mark I self-shielded ^{137}Cs irradiator at a dose rate of 1.61 Gy/min. For preliminary experiments using parental COV434 cells, trypsinized cells were suspended in complete

media in 15-ml conical tubes, irradiated and then plated for subsequent assays. In subsequent experiments, cells were plated and irradiated 24 h or more later. For water-soluble tetrazolium (WST)-1 assays, plating media were removed from the wells of a 96-well microplate and replaced with 30 μl DMEM–F12; after irradiation, media volumes were completed to 100 μl. For terminal deoxynucleotidyl transferase-mediated deoxyuridine triphosphate nick-end-labelling (TUNEL) assay, plating media were removed from the chambers of Nunc Lab-Tek II CC2 8-Chambered Slide System and replaced with 90 μl DMEM–F12; after irradiation, media volumes were completed to 200 μl. For caspase 3 immunoblotting, plating media were removed from 25-cm^2 flasks and replaced with 5 ml DMEM–F12 prior to irradiation. For the experiment in which GSH was suppressed with BSO, cells were irradiated in six-well plates after culture for 24 h with medium containing 0, 1, 5 or 100 μM BSO without removing the medium. These doses were chosen to cause varying degrees of GSH suppression from <50% to >85% suppression based on preliminary experiments in COV434 cells.

WST-1 assay

Cell metabolic activity, an indicator of cell viability, was measured based on the cleavage of a WST-1 salt to formazan by mitochondrial dehydrogenases of viable granulosa cells. For WST assays, 1×10^4 live cells were plated per well of a 96-well tissue culture-treated microplate. For the experiments in Figures 5 and 8, cells were treated with H_2O_2 or gamma irradiation directly in the plate. For the experiments in Figure 6, cells were trypsinized and suspended in medium, irradiated while in suspension and then plated for the assay. At the end of the treatment periods, 10 μl of WST-1 reagent was pipetted into each well, and the plates were incubated for 2 h at 37°C. Blank wells contained culture medium and WST-1 reagent with no cells. The absorbance at 440 nm was then read using a VersaMax Tunable Microplate Reader (Molecular Devices). WST-1 cleavage to a formazan results in a colour change. The absorbance at 440 nm is therefore proportional to the number of viable cells. The average of the blank absorbance values was subtracted from the absorbance reading for each well and the resulting values were used for data analysis.

2′,7′-Dichlorofluorescin diacetate assay to detect ROS

ROS were measured using the cell permeable compound, 2′,7′-dichlorofluor-escin diacetate (H_2DCF-DA; Molecular Probes, Eugene, OR). H_2DCF-DA is taken up by cells, where it is cleaved by cytosolic esterases to the non-fluorescent compound dichlorofluorescin, which in the presence of various ROS and nitrogen species is oxidized to the fluorescent compound, dichlorofluorescein (DCF) (43,44).

In preliminary experiments, suspensions of the parental COV434 cells were irradiated with 0, 1 or 5 Gy and then plated in six-well tissue culture plates. After 6, 24 or 48 h, conditioned media were removed, and 10 μM H_2DCF-DA in fresh media was added. Cells were incubated for 30 min, washed, trypsinized and resuspended in the conditioned media. DCF fluorescence was then immediately measured using fluorescence-activated cell sorting (45).

For subsequent experiments, a previously described H_2DCF-DA microplate assay was used (35,46). In total, 2×10^4 live cells per well of a 96-well tissue culture-treated, black-sided microplate were incubated for 24 h. Cells were then irradiated with 0, 1 or 5 Gy. After irradiation and just prior to the addition of H_2DCF-DA, positive control COV434 cells were treated for 30 min with 0.5 mM H_2O_2. At 0.5, 2 or 6 h after irradiation, media were removed and replaced with media containing 100 μM H_2DCF-DA. Negative control wells received media without H_2DCF-DA. Cells were incubated for 30 min. The H_2DCF-DA-containing medium was then removed; cells were washed with PBS and maintained in PBS while fluorescence intensity was read using a GENios Plus Multi-Detection Microplate Reader with Enhanced Fluorescence (Tecan Group) with excitation wavelength set at 485 nm and emission wavelength set at 535 nm. Three separate experiments were performed.

TUNEL assay

Apoptosis was detected in irradiated cells using the *In Situ* Cell Death Detection Kit, POD (Roche Molecular Biochemicals, Mannheim, Germany), as previously described (35,47). Cells were cultured at 5×10^4 per chamber of a Nunc Lab-Tek II CC2 8-Chambered Slide for 24 h, irradiated with 0, 1 or 5 Gy and returned to the incubator. After 2 or 6 h, cells were washed with ice-cold PBS and fixed with 4% paraformaldehyde for 30 min on ice. Slides were washed in PBS, treated with 3% hydrogen peroxide in methanol for 10 min, washed in PBS, permeabilized with 0.1% Triton X-100 in 0.1% sodium citrate for 2 min on ice, washed, blocked for 30 min at room temperature with 3% BSA in PBS, washed, incubated at 37°C for 1 h with terminal deoxynucleotidyl transferase/label solution (containing fluorescein-labelled deoxyuridine triphosphate) and washed again. Positive control slides were treated with DNAse I (500 U) prior to labelling, and the terminal transferase was omitted for negative control slides. Slides were then blocked with 3% BSA in PBS,

washed, incubated for 30 min at 37°C with peroxidase converter solution (anti-fluorescein antibody, Fab fragment from sheep, conjugated with horseradish peroxidase) and diluted 1.5:1 in TUNEL dilution buffer. Slides were then washed and incubated for 5 min with diaminobenzidine substrate solution (Roche Molecular Biochemicals), washed in PBS and counterstained with haematoxylin. All washes and incubations were at room temperature unless otherwise indicated. Data from two separate experiments were pooled for analysis. The numbers of TUNEL-positive and TUNEL-negative cells in three ×400 microscopic fields per well were counted by an observer blind to treatment and genotype. The average of the counts was used for data presentation and statistical analyses.

Statistical analyses

Data from two or three replicate experiments were pooled for statistical analyses unless otherwise noted. Homogeneity of variances was assessed by Levene's test. Data expressed as proportions (percentages of TUNEL-positive cells) were subjected to arcsine square root transformations prior to analysis (48). The differences among groups were analysed by analysis of variance (ANOVA) followed by Fisher's least significant difference (LSD) test. When variances were non-homogeneous, the Kruskal–Wallis test for non-parametric data was used. If the Kruskal–Wallis test was significant at $P < 0.05$, the Mann–Whitney test was then used for intergroup comparisons. Statistical analyses were carried out using SPSS 16.0 for Mac OS X.

Results

Transgenes were stably integrated into the genomic DNA of transfected COV434 cells

Genomic DNA from all stably transfected cell lines was genotyped using CMVGCLC-PCR and/or CMVGCLM-PCR to confirm that the cells had stably integrated the correct transgenes. Figure 1 shows examples of cell lines that had and had not stably integrated the correct transgenes, as dictated by the vectors used during the transfection process (pCMV-Script control vector, pCMVGCLC-Script vector, pCMVGCLM vector or both the pCMVGCLC-Script and the pCMVGCLM vectors). In this and subsequent sections, cell lines transfected with both pCMVGCLC-Script vector and pCMVGCLM vector are designated 'CM' followed by a number and lower case letter, cell lines transfected with pCMVGCLC-Script vector only are designated 'C' followed by a number and lower case letter and cell lines transfected with pCMVGCLM vector only are designated 'M' followed by a number and letter. The empty vector-transfected control cells are designated CMV9b. Cell lines CM4b and CM3a did not appear to integrate the CMVGCLC transgene, but both did have very light bands corresponding to the CMVGCLM transgene. The remaining cell lines integrated the transgenes with which they were transfected.

COV434 cells stably transfected with Gclc, Gclm or both GCL subunits display varying concentrations of total intracellular GSH

Figure 2 shows the total GSH concentrations in the parental and stably transfected cell lines. GSH levels varied significantly by cell genotype whether expressed as nanomole per 10^6 cells or nanomole per milligram protein ($P < 0.001$ by Kruskal–Wallis test). When expressed as nanomole GSH per 1×10^6 cells, parental COV434 cells displayed virtually the same GSH levels as control cells transfected with empty pCMV-Script vector, the CMV9b cells (7.2 ± 0.3 and 6.6 ± 0.5 nmol GSH/1×10^6 cells, respectively). The cell lines CM2a, CM4b, C5a, C6a, C6b and M5a displayed statistically significantly higher total GSH levels relative to COV434 parental cells and CMV9b control cells ($P < 0.04$ and $P < 0.03$, respectively, by Mann–Whitney tests; Figure 2A). GSH concentrations were 1.8-fold higher in CM2a cells,
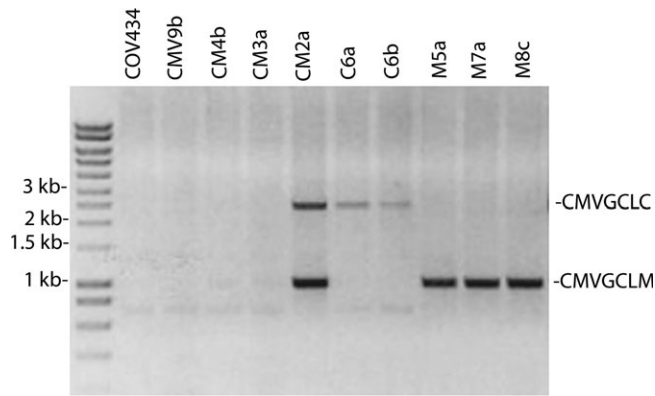
Fig. 1. Transgene-specific CMVGCLC-PCR and CMVGCLM-PCR were used to confirm stable integration of transgenes into genomic DNA of transfected COV434 cells. COV434 refers to the parental cell line. CMV9b refers to a cell line stably transfected with pCMV-Script vector. All cell lines stably transfected with a 1:1 molar ratio of pCMVGCLC-Script and pCMVGCLM vectors are designated CM followed by a number and lower case letter (e.g. CM4b, CM3a and CM2a). All cell lines stably transfected with pCMVGCLC-Script vector are designated C followed by a number and lower case letter (e.g. C6a and C6b). All cell lines stably transfected with pCMVGCLM vector are designated M followed by a number and lower case letter (e.g. M5a, M7a and M8c). The amplified product corresponding to the CMVGCLC transgene is 2.44 kb, while the amplified product corresponding to the CMVGCLM transgene is 1.112 kb. Cell lines CM4b and CM3a did not integrate the CMVGCLC transgene, but displayed faint bands corresponding to integration of the CMVGCLM transgene. The remaining cell lines integrated the transgenes with which they were transfected.

1.3-fold higher in CM4b cells, 1.6-fold higher in C5a cells, 2.4-fold higher in C6a cells, 1.9-fold higher in C6b cells and 1.7-fold higher in M5a cells than in control CMV9b cells when expressed as nanomole GSH per 1×10^6 cells. The cell lines C3b, C6c, M7a and M8c did not display statistically significant differences in total GSH concentrations relative to either COV434 parental cells or CMV9b control cells (Figure 2A). The cell line CM3a displayed a statistically significant decrease of 33% in total GSH levels relative to parental COV434 cells ($P = 0.002$ by Mann–Whitney test), but not CMV9b cells (Figure 2A). When total intracellular GSH levels were expressed as nanomole GSH per milligram protein, the results followed the same trends as the data described above, although the results of statistical analyses varied somewhat (Figure 2B).

Because CM2a, C6a, C6b and M5a cells displayed statistically significant increases in total GSH relative to control CMV9b cells and had stably integrated the transgenes by PCR, these cells were selected for use in subsequent experiments in which cells were challenged with H_2O_2 or ionizing radiation.

Stably transfected cells display increased GCLC and/or GCLM protein expression

GCLC and GCLM protein levels varied in a statistically significant manner with genotype ($P = 0.001$ and $P < 0.001$ by Kruskal–Wallis tests, respectively, Figure 3). Control CMV9b cells had virtually the same GCLC and GCLM protein levels as parental COV434 cells (1.3- and 0.9-fold COV434 controls, respectively). CM2a cells co-transfected with *Gclc* and *Gclm* displayed a statistically significant increase in GCLC protein expression levels of 1.5-fold relative to parental COV434 controls ($P = 0.040$ by Mann–Whitney test) and a small, statistically non-significant increase relative to CMV9b controls. They also had small, non-statistically

significant increases in GCLM levels relative to both COV434 and CMV9b controls (Figure 3). C6a cells transfected with *Gclc* had statistically significant increases in GCLC protein expression of 14.9-fold relative to COV434 control cells ($P < 0.001$ by non-parametric Mann–Whitney test) and 11.5-fold relative to CMV9b controls ($P < 0.001$). C6b cells transfected with *Gclc* had 8-fold increases in GCLC in an initial experiment, but did not show any increase in GCLC levels in a subsequent experiment, suggesting that copies of the transgene were lost over time. As a result, the pooled data for C6b cells from all experiments showed a non-significant increase in GCLC protein levels of 4.6-fold over COV434 control cells. In contrast, C6b cells consistently showed a reproducible and statistically significant decrease in GCLM protein expression of 0.3-fold relative to COV434 control cells ($P = 0.017$ by Mann–Whitney test). M5a cells transfected with *Gclm* had statistically significant increases in GCLM protein expression of 3.5-fold relative to COV434 controls ($P = 0.008$ by Mann–Whitney test) and 4-fold relative to CMV9b controls ($P = 0.001$).

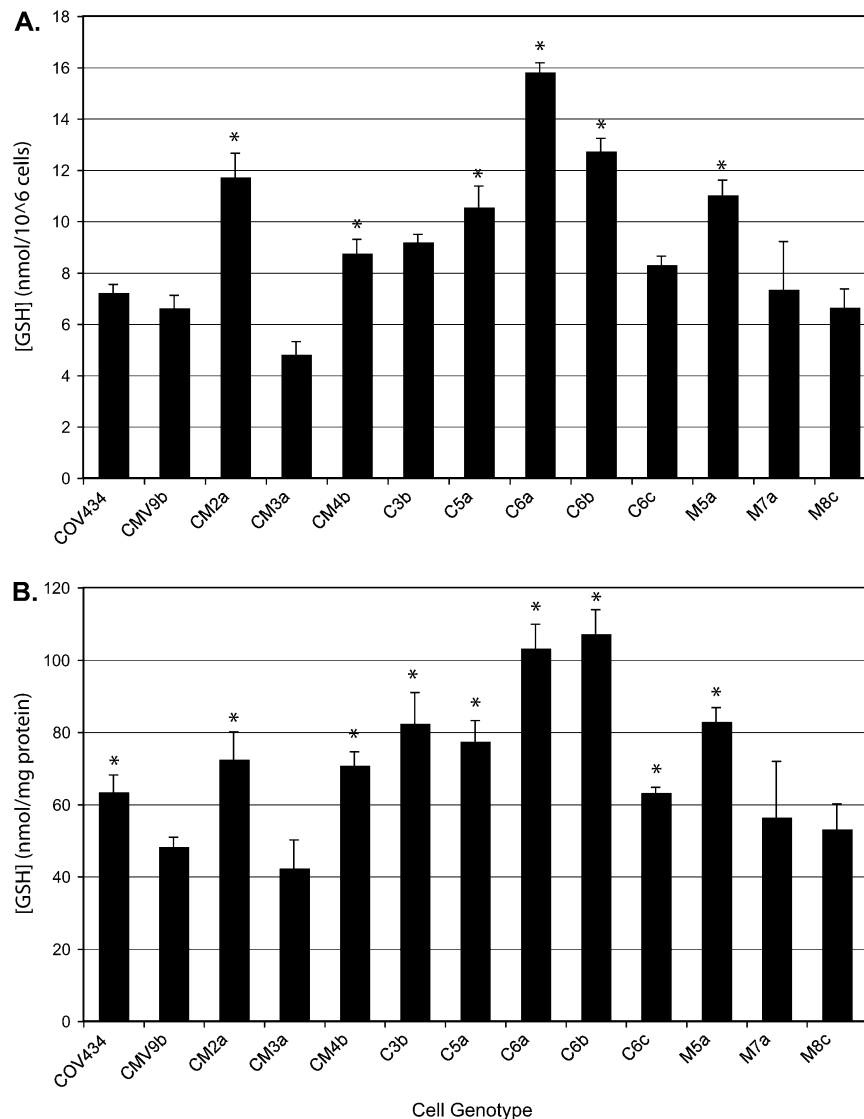*Stable transfection of COV434 granulosa cells with Gclc and/ or Gclm increased GCL enzymatic activity*

GCL enzymatic activity varied in a statistically significant manner with genotype ($P < 0.001$ by one-way ANOVA; Figure 4). Parental COV434 cells and control CMV9b cells had virtually the same GCL activity levels (0.134 ± 0.011 and 0.142 ± 0.011 nmol GSH/mg protein/min, respectively). GCL enzymatic activity increased by 2.0-fold in CM2a cells transfected with both *Gclc* and *Gclm* relative to CMV9b cells ($P < 0.001$ by LSD test). C6a cells transfected with *Gclc* also displayed a statistically significant increase in GCL enzymatic activity of 2.8-fold when compared to CMV9b cells ($P < 0.001$ by LSD test). C6b and M5a cells displayed small, statistically insignificant increases in GCL enzymatic activity when compared to either COV434 or CMV9b cells.

Overall, the changes in GCLC and GCLM protein expression, GCL enzymatic activity and GSH concentrations in the stably transfected cell lines are consistent with one another, with C6a cells transfected with *Gclc* having the greatest fold increases in GCLC protein levels, GCL enzymatic activity and GSH levels.

Stable transfection of COV434 granulosa cells with GCL subunits increased resistance to hydrogen peroxide-induced cell death

Cells were treated with various concentrations of H_2O_2 for 30 min to induce oxidative stress and then assayed for metabolic activity based on the cleavage of WST-1. For all cell genotypes, metabolic activity decreased in a concentration-dependent manner with H_2O_2 treatment (Figure 5A). The effects of H_2O_2 concentration and genotype were statistically significant by two-way ANOVA ($P < 0.001$ and $P = 0.003$, respectively); however, because variances were not homogeneous, non-parametric tests were used for subsequent comparisons. The effect of cell genotype on metabolic activity was statistically significant at every concentration, except 1 mM H_2O_2 ($P \leq 0.001$ by Kruskal–Wallis tests at each concentration; Figure 5A). At all concentrations, excluding 1 mM H_2O_2, C6a and C6b *Gclc*-transfected cells had significantly higher WST-1 cleavage than COV434 and CMV9b control cells (Figure 5A). At all H_2O_2 concentrations, the differences in metabolic activity between parental COV434 and control

A.

B.

Cell Genotype

Fig. 2. Overexpression of *Gclc* and/or *Gclm* in COV434 human granulosa cells increases intracellular GSH concentrations. Total intracellular GSH was measured in stably transfected cells and expressed as nanomole GSH per 10^6 cells (**A**) or nanomole GSH per milligram protein (**B**). The graphs show the mean + SEM of the GSH concentrations. GSH concentrations varied significantly with genotype ($P < 0.001$ by Kruskal–Wallis test). *Significantly different from CMV9b by Mann–Whitney test, $P < 0.05$; $n = 3$–17 per genotype.

CMV9b cells were negligible and not statistically significant (Figure 5A).

Cells were also treated with 0.5 mM H_2O_2 and then similarly assayed for metabolic activity at various times after treatment. The effect of genotype on metabolic activity was statistically significant at every time point ($P < 0.001$ by Kruskal–Wallis tests; Figure 5B). For all cell genotypes, granulosa cell metabolic activity decreased with H_2O_2 treatment. Control cells showed a time-dependent decrease in metabolic activity until the 2-h time point after which metabolic activity reached a plateau. All GCL-transfected cells showed decreases in metabolic activity with H_2O_2 treatment, but after 1 h, the cells recovered and metabolic activity began to increase (Figure 5B). At all treatment times, the cell lines that had been stably transfected with *Gclc* and/or *Gclm* (C6a, C6b, CM2a and M5a) had statistically significantly smaller decreases in metabolic activity than did the CMV9b control cells. The greatest protective effect of overexpression of GCL subunits was observed in the C6a cell line, which had the highest

intracellular GSH concentrations. At all treatment time points, the differences in WST-1 cleavage between parental COV434 and control CMV9b cells were smaller than differences between either control cell line and any of the GCL subunit-overexpressing cell lines.

Taken together, the H_2O_2 dose–response data and H_2O_2 time course data suggest that the *Gclc*- and *Gclm*-transfected granulosa cells, due to their increased ability to synthesize GSH, are able to respond to and overcome the oxidant insults. These results support the hypothesis that GSH is involved in protecting granulosa cells against ROS-mediated cell death.

Treatment with ionizing radiation led to increases in ROS and cell death in COV434 granulosa cells

In a preliminary experiment to select the optimal radiation doses for subsequent experiments, parental COV434 cells were irradiated with 0, 1, 2, 5 or 10 Gy and metabolic activity was measured at 48, 72 and 96 h after irradiation (Figure 6A). At all time points, there was a dose-dependent decrease in metabolic
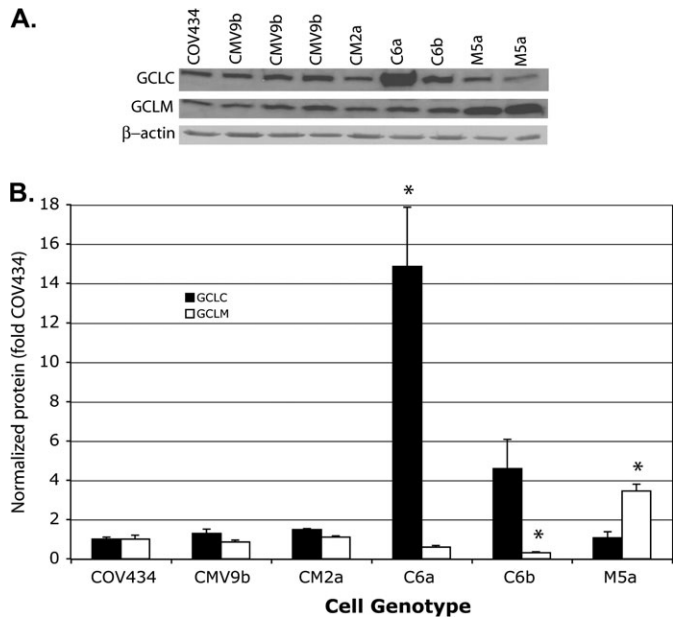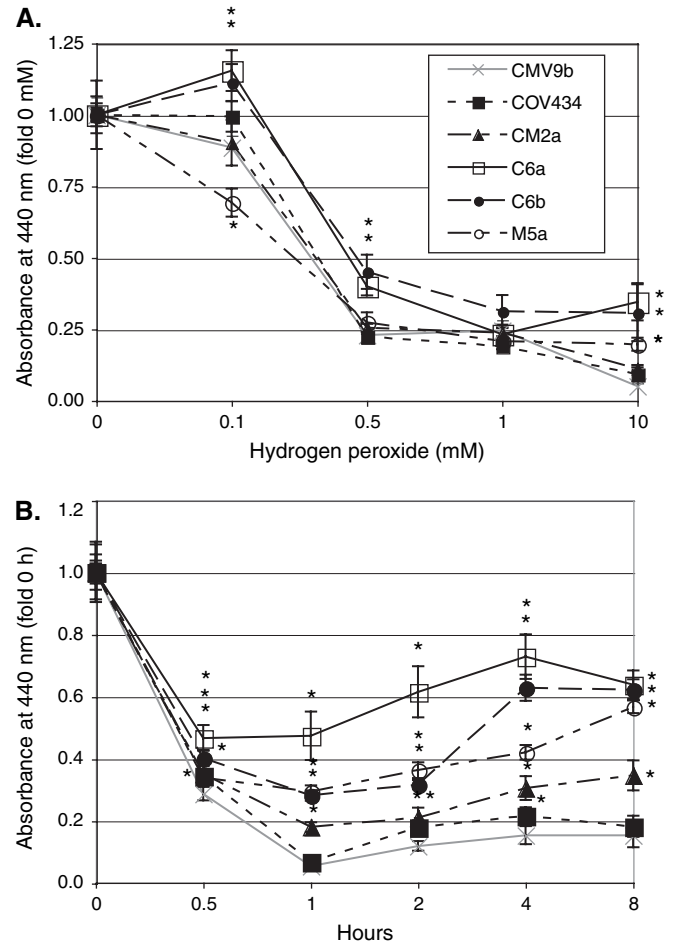
Fig. 3. Overexpression of *Gclc* and/or *Gclm* in COV434 human granulosa cells increases GCLC and GCLM protein levels. See Figure 1 for an explanation of the genotype designations. GCLC and GCLM protein levels were determined by immunoblotting. (**A**) Representative immunoblot showing GCLC, GCLM and β-actin in parental COV434 and stably transfected cell lines. (**B**) The graph shows the mean + SEM of the GCLC and GCLM absorbances normalized to β-actin absorbance and expressed as fold the COV434 cell level for a given blot. Total GCLC and GCLM protein levels varied in a statistically significant manner with genotype ($P = 0.001$ and $P < 0.001$, respectively, by Kruskal–Wallis test). *Significantly different from CMV9b by Mann–Whitney test, $P < 0.01$; $n = 2$–11 per genotype.
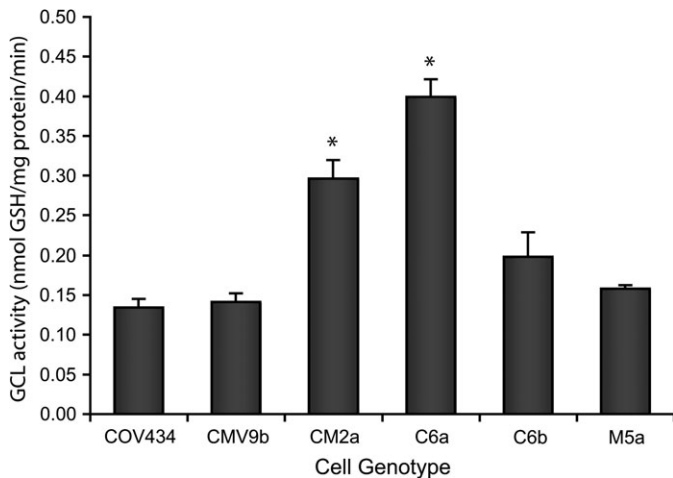
Fig. 4. Overexpression of *Gclc* and/or *Gclm* in COV434 human granulosa cells increases GCL enzymatic activity. See Figure 1 for an explanation of the genotype designations. The graph shows the mean + SEM of the GCL activity. The GCL activity varied in a statistically significant manner with genotype ($P < 0.001$, one-way ANOVA). *Significantly different from CMV9b by LSD test, $P < 0.001$; $n = 4$–6 per genotype.

activity, with significant decreases in the number of viable cells observed at all doses compared to controls ($P < 0.001$, effect of dose by Kruskal–Wallis test at all times). To begin to test whether ROS may play a role in radiation-induced cell death in granulosa cells, COV434 cells were irradiated with 0, 1 or 5 Gy, and ROS were measured as DCF fluorescence after 6, 24 and 48 h. DCF fluorescence increased in a dose-dependent


Fig. 5. Overexpression of *Gclc* and/or *Gclm* in COV434 human granulosa cells protects against H_2O_2-induced cell death. See Figure 1 for an explanation of the genotype designations. (**A**) Cells were treated with the indicated concentrations of H_2O_2 for 30 min, and cell metabolic activity was then assessed by WST-1 tetrazolium assay. (**B**) Cells were treated with 0.5 mM H_2O_2 for the indicated lengths of time and subjected to WST-1 assay. The graphs show the mean ± SEM of the cleaved WST-1 absorbance expressed as fold the 0-mM control for that genotype (**A**) or as fold the 0-h control for that genotype (**B**). (**A**) The effect of genotype was statistically significant at all doses of H_2O_2 except 1 mM ($P \leq 0.001$ by Kruskal–Wallis test). *Significantly different from CMV9b control at same concentration by Mann–Whitney test, $P < 0.05$. (**B**) The effect of genotype was statistically significant at all times after onset of H_2O_2 treatment ($P \leq 0.001$ by Kruskal–Wallis test). *Significantly different from CMV9b control at same time point by Mann–Whitney test, $P < 0.05$.

manner at all time points ($P < 0.04$ by Kruskal–Wallis test; Figure 6B). Because there was a significant increase in ROS generation observed after radiation treatment of the parental cells, we hypothesized that GCL-transfected cells would be protected when irradiated much like they were protected against H_2O_2 treatment. Because there was a significant increase in ROS generation already 6 h after radiation treatment, we chose to focus on the early, acute effects of radiation treatment in subsequent studies of ROS generation and apoptotic end points.

Stable transfection of COV434 granulosa cells with Gclc attenuated radiation-induced generation of ROS

We tested the effects of GCL overexpression on the generation of ROS after gamma irradiation using DCF fluorescence (Figure 7). The effects of radiation dose, time since irradiation
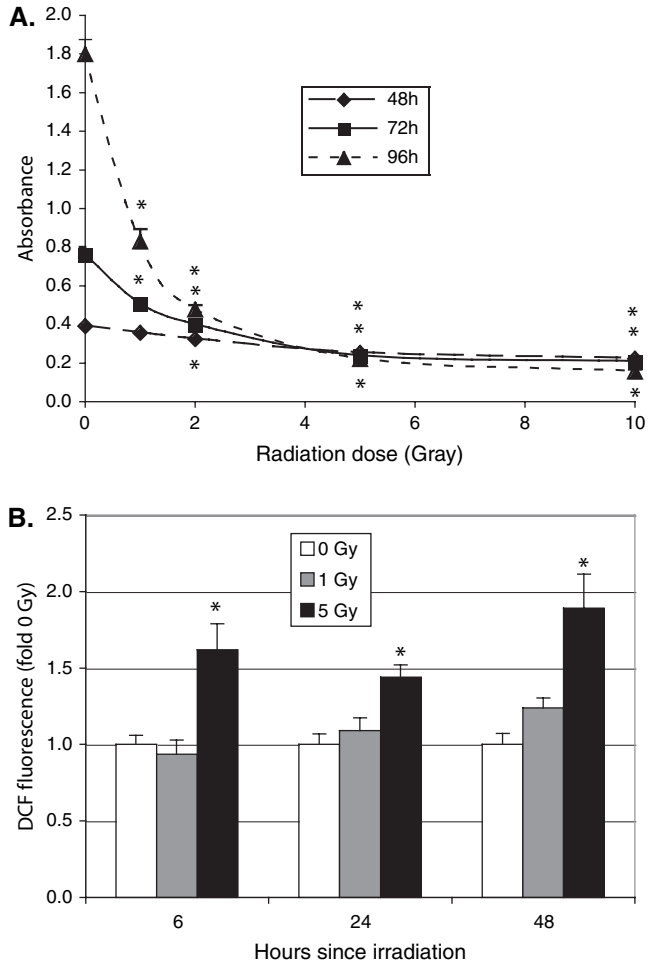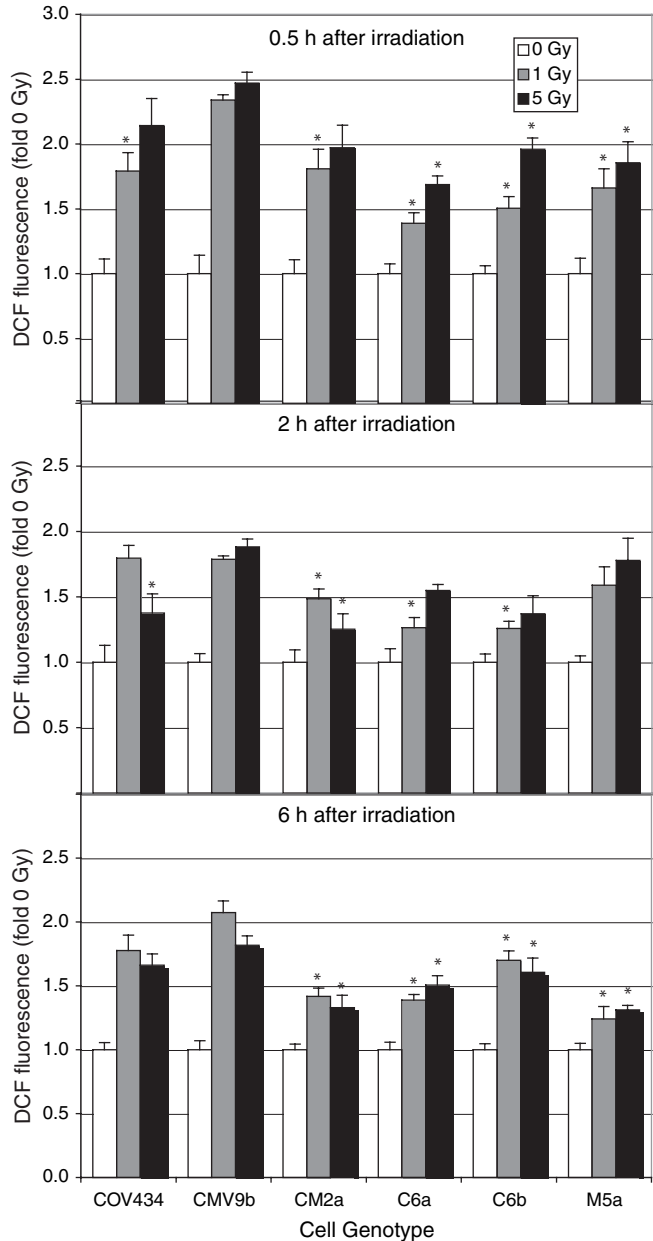
Fig. 6. Gamma irradiation induces cell death and generates ROS in human granulosa cells. Parental COV434 cells were irradiated while suspended in medium with 0, 1, 2, 5 or 10 Gy, then plated and cultured for the indicated periods of time. (**A**) Cell metabolic activity in irradiated COV434 cells was assessed using the WST-1 tetrazolium assay. WST absorbance was dose-dependently decreased with gray of radiation at all time points after irradiation ($P < 0.001$, effect of dose by Kruskal–Wallis test at all time points). *$P < 0.01$ versus respective 0-Gy control by Mann–Whitney test. (**B**) At the indicated times, cells were trypsinized and subjected to measurement of DCF fluorescence, an indicator or ROS, by flow cytometry. DCF fluorescence was significantly increased at all three time points after irradiation ($P < 0.04$, effect of dose by Kruskal–Wallis test). *$P = 0.021$ versus respective 0-Gy control by Mann–Whitney test.

Fig. 7. Overexpression of *Gclc* and/or *Gclm* results in diminished ROS generation by human granulosa cells in response to ionizing radiation. See Figure 1 for an explanation of the genotype designations. Cells were plated in 96-well microplates and were irradiated with the indicated doses of gamma rays. At 0.5, 2 or 6 h after irradiation, ROS were measured using DCF fluorescence. The graphs show the mean + SEM DCF fluorescence expressed as fold the 0-Gy control fluorescence for that genotype and time point. For each genotype at each time point, there was a dose-dependent increase in ROS ($P < 0.01$ by Kruskal–Wallis test). For each dose and time point, the rise in ROS varied by cell genotype ($P < 0.01$ by Kruskal–Wallis test). *Significantly different from control CMV9b cells at same time point and radiation dose, $P < 0.05$ by Mann–Whitney test; $n = 9$ per group.

and genotype were statistically significant (all $P < 0.001$ by three-way ANOVA). However, since the variances were not homogeneous, subsequent comparisons were made using non-parametric tests. When cells were irradiated with 1 or 5 Gy, all cell genotypes demonstrated increases in ROS relative to sham-irradiated controls of the same genotype after 0.5, 2 and 6 h ($P < 0.01$, effect of dose for all genotypes and time points by Kruskal–Wallis test).

Irradiated cells displayed a genotype-specific response in ROS generation. ROS levels varied in a statistically significant manner by genotype for both the 1- and the 5-Gy doses at all time points ($P \leq 0.01$ by Kruskal–Wallis test). At all three time points after both doses of gamma irradiation, the CMV9b control cells had the highest relative increases in ROS levels, and one or more of the GCL subunit-overexpressing cell lines had statistically significantly lower ROS generation than the control CMV9b cells (Figure 7). The *Gclc*-overexpressing C6a cells,

which had the highest GSH concentrations, also had the greatest attenuation of ROS generation relative to the CMV9b controls.

Stable transfection of COV434 granulosa cells with Gclc increased resistance to radiation-induced cell death

We tested the effects of overexpression of GCL subunits on radiation-induced cell death using the WST-1 metabolic activity assay. We observed significant effects of radiation

dose, treatment time and cell genotype on metabolic activity ($P < 0.001$ by three-way ANOVA for all comparisons). However, since the variances were not homogeneous, subsequent comparisons were made using non-parametric tests.

The fold increase in metabolic activity relative to 0 h varied with cell genotype at both the 72- and the 96-h time points and for all three doses of radiation ($P < 0.009$ by Kruskal–Wallis test). All cell genotypes demonstrated cellular proliferation, despite having been treated with 1 Gy of γ-rays, as indicated by the increase in the number of viable cells over time (Figure 8). In contrast, only the C6a and C6b cells, which overexpressed *Gclc*, and the control CMV9b cells demonstrated any proliferation, albeit very reduced, after treatment with 5 Gy (Figure 8). After 96 h and despite being irradiated with 5 Gy,

C6a and C6b cells displayed statistically significant, ∼2-fold increases in the numbers of viable cells relative to their initial numbers at 0 h ($P < 0.001$, effect of time by Kruskal–Wallis test; $P < 0.001$, 96 versus 0 h by Mann–Whitney test). While the CMV9b controls demonstrated a small 1.3-fold increase over 0 h levels at 96 h ($P = 0.004$ by Mann–Whitney test), the differences between the C6a and C6b lines and the CMV9b line at 96 h were statistically significant ($P < 0.001$ by Mann–Whitney test). The 5-Gy-irradiated COV434 and CM2a cells, on the other hand, displayed significantly smaller fold increases than CMV9b controls at 96 h ($P = 0.005$ and $P = 0.037$ by Mann–Whitney tests, respectively).

Interestingly, the effect of cell genotype on cellular proliferation was also statistically significant in untreated
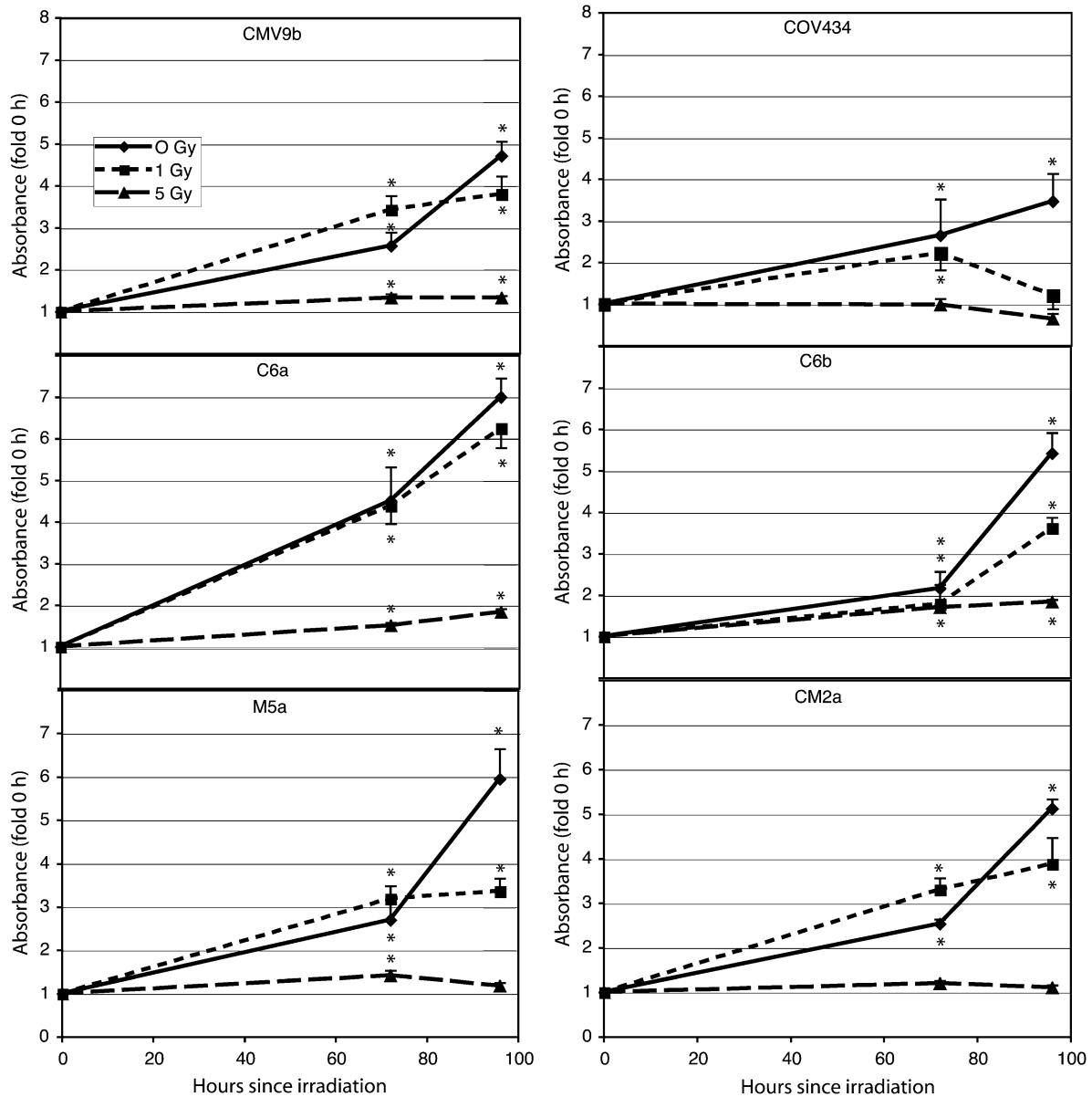
Fig. 8. Overexpression of *Gclc* and/or *Gclm* protects human granulosa cells against cell death after treatment with ionizing radiation. Cells were irradiated with 1 or 5 Gy or were sham irradiated in 96-well plates and cell metabolic activity was assessed by WST-1 assay. Results from a representative experiment are shown ($n = 3$–10 wells per group). The experiment was repeated three times, with similar results each time. The graphs show the mean ± SEM of the cleaved WST-1 absorbance expressed as fold the 0-h level for each cell line. Metabolic activity increased significantly with time for all genotypes at the 0- and 1-Gy doses and for the CMV9b, C6a, C6b and M5a cell lines at 5 Gy ($P < 0.03$, effect of time by Kruskal–Wallis test; *$P < 0.05$ relative to 0 h for same dose and genotype by Mann–Whitney test), but not for the COV434 and CM2a cell lines at the 5-Gy dose. The fold increase in metabolic activity relative to 0 h varied with cell genotype at both the 72- and 96-h time points and for all three dose groups ($P < 0.009$, effect of genotype by Kruskal–Wallis test).

(0 Gy) cells at both 72 and 96 h ($P < 0.008$ by Kruskal–Wallis test). *Post hoc* analysis by Mann–Whitney test revealed that only the *Gclc*-overexpressing C6a cells had statistically significant fold increases in viable cells relative to the CMV9b controls at 72 and 96 h ($P < 0.01$ by Mann–Whitney test). All other untreated cells displayed no statistically significant differences relative to CMV9b controls at either time point.

These results suggest that *Gclc* overexpression protects cells against radiation-induced cell death, as well as conferring a growth advantage to cells growing in culture in the absence of exposure to radiation. C6a cells, the stably transfected cell line with the greatest increase in intracellular GSH, were most protected against the deleterious effects of γ-rays. Together with the observation that C6a cells also demonstrated the greatest attenuation in ROS generation in response to irradiation, these results led us to select C6a cells for further studies. We have previously shown that treatment of parental COV434 cells with the alkylating agent cyclophosphamide resulted in ROS generation, followed by apoptosis. We hypothesized that the increase in ROS in response to γ-rays would similarly lead to the initiation of apoptosis and that C6a cells would be protected against this effect.

Stable transfection of COV434 granulosa cells with Gclc protected against radiation-induced apoptosis

We used TUNEL assay and activated caspase-3 immunodetection to test the hypothesis that overexpression of *Gclc* would protect human granulosa cells against the induction of apoptosis by ionizing radiation. The percentage of TUNEL-positive cells increased in a dose-dependent manner for the control CMV9b and COV434 cells, as well as for the *Gclc*-overexpressing C6a cells (Figure 9). The increase in TUNEL-positive cells was already evident at 2 h and became pronounced at 6 h after irradiation (Figure 9A). The effects of genotype, radiation dose and treatment time, as well as of the two-way and three-way interactions among those variables, on the arcsine square root-transformed fraction of TUNEL-positive cells were statistically significant by three-way ANOVA ($P < 0.001$ for all effects). Because the variances were not homogeneous, non-parametric tests were used for subsequent comparisons. The effect of genotype was statistically significant for the 5-Gy dose at 2 h and for both the 1- and the 5-Gy doses at 6 h ($P < 0.02$ by Kruskal–Wallis test). The *Gclc*-overexpressing C6a cells had significantly fewer TUNEL-positive cells 2 h after the 5-Gy dose and 6 h after both the 1- and the 5-Gy doses than either control CMV9b or COV434 cells ($P < 0.02$ by Mann–Whitney test).

The increase in TUNEL-positive apoptotic cells was associated with activation of caspase 3, which is indicated by the appearance of cleaved 17- and 19-kDa activated forms of the enzyme (Figure 9B). Cleaved caspase 3 bands were not visible in control CMV9b or COV434 cells or in *Gclc*-overexpressing C6a cells at 2 h after irradiation (data not shown). By 6 h after irradiation, cleaved caspase 3 was clearly evident in the two control cell lines and was still absent in the C6a cells (Figure 9B).
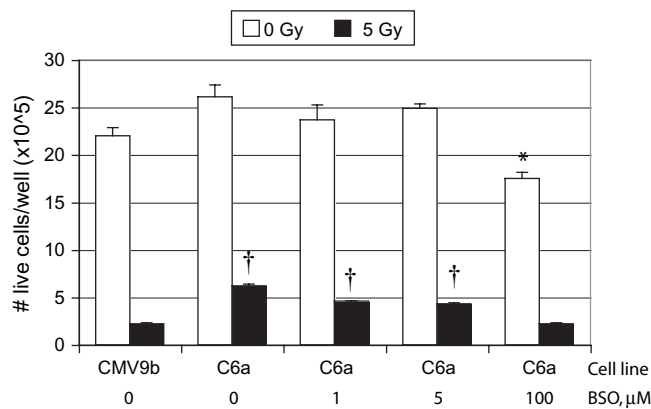
Suppression of GSH synthesis reversed the protective effect of Gclc overexpression against ionizing radiation on COV434 cells

To test whether the protective effect of stable transfection with *Gclc* is due to increased GSH synthesis, GSH synthesis was biochemically suppressed with BSO, an inhibitor of GCL
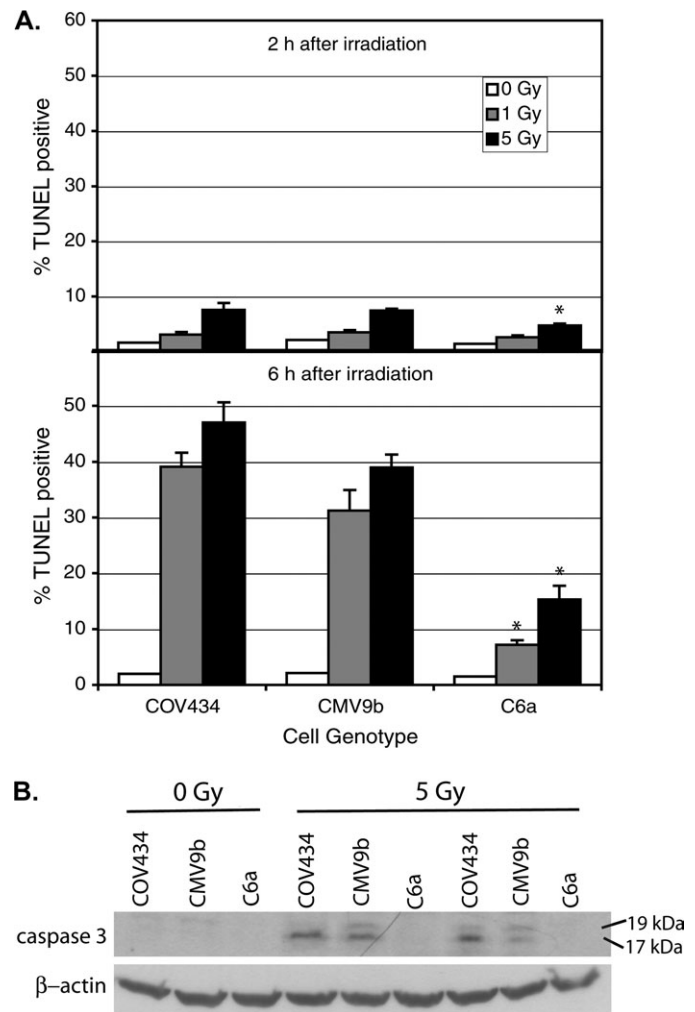
Fig. 9. Overexpression of *Gclc* and/or *Gclm* protects human granulosa cells against the induction of apoptosis by ionizing radiation. Cells were cultured in chambered tissue culture slides (**A**) or in 25-cm² flasks (**B**) and were irradiated with 5-Gy gamma rays or were sham irradiated. (**A**) Mean + SEM percentage of TUNEL-positive apoptotic cells at the indicated times after irradiation (pooled results from two experiments, $n = 4$–6 per group). The percentage of TUNEL-positive cells increased in a dose-dependent manner for all three genotypes at 2 and 6 h ($P < 0.02$, effects of dose by Kruskal–Wallis test). The effect of genotype was statistically significant for the 5-Gy dose at 2 h and for both the 1- and the 5-Gy doses at 6 h ($P < 0.02$ by Kruskal–Wallis test). *Significantly different from CMV9b or COV434 control at same dose and time, $P < 0.02$ by Mann–Whitney test. (**B**) Representative western blot showing caspase 3 activation (caspase 3 cleavage products at 17 and 19 kDa) in empty vector-transfected control CMV9b cells and parental COV434 cells at 6 h after irradiation with 5 Gy and no caspase 3 activation in irradiated C6a cells overexpressing *Gclc*.

activity. C6a cells were treated with 0, 1, 5 or 100 μM BSO for 24 h prior to 5-Gy irradiation or sham irradiation; control CMV9b cells were also irradiated but not treated with BSO. Three days after irradiation or sham irradiation, cells were trypsinized and live cells were counted using trypan blue exclusion. As shown in Figure 10, suppression of GSH synthesis in the *Gclc*-overexpressing C6a cells with increasing doses of BSO dose-dependently increased sensitivity to ionizing radiation. The C6a cells treated with 100 μM BSO were as sensitive to 5-Gy radiation as the control CMV9b cells ($P = 1.00$; C6a, 100 μM BSO versus CMV9b, 0 μM BSO by Tukey's honestly significant difference (HSD) *post hoc* test).

Fig. 10. Biochemical suppression of GSH synthesis with BSO reverses the protective effect of overexpression of *Gclc* against ionizing radiation. C6a or CMV9b cells were cultured in six-well plates for 24 h with the indicated doses of BSO and were then irradiated with 5-Gy gamma rays or were sham irradiated. After three more days of culture in media containing BSO or control media, the cells were trypsinized, and live cells were counted by trypan blue exclusion. The graph shows the mean + SEM live cells per well ($n = 3$–4 wells per group). The effect of radiation dose was statistically significant by two-way ANOVA ($P < 0.001$). Within radiation dose, the effect of treatment group was statistically significant by one-way ANOVA ($P < 0.001$; *different from CMV9b, 0 Gy by *post hoc* Tukey's HSD test, $P < 0.05$. †Different from CMV9b, 5 Gy by *post hoc* Tukey's HSD test, $P < 0.001$).

Discussion

Radiation therapy can damage ovarian follicles and cause temporary or permanent infertility. Radiation can also indirectly damage cells by generating ROS that can persist for various times post-irradiation. The redox environment is critical to intracellular homoeostasis and has been shown to be important in the progression of programmed cell death. Herein, we showed for the first time that ionizing radiation treatment generates ROS and subsequently causes apoptotic death in cultured human granulosa cells. GSH is an important antioxidant, and its synthesis has been shown to be upregulated in radiation-resistant cancer cells. Our results show that stable overexpression of one or both subunits of GCL, the rate-limiting enzyme in GSH synthesis, in a human granulosa tumour cell line enhances GSH synthesis and protects the cells against hydrogen peroxide and ionizing radiation-induced cell death. Our novel findings demonstrate how strategies aimed at manipulating GSH levels can modulate radiation-induced granulosa cell apoptosis.

Radiation therapy, together with chemotherapy, has greatly enhanced the survival rates of young women afflicted with various forms of malignant cancers. Destruction of ovarian follicles, leading to infertility, is an unfortunate side effect of such aggressive treatments that can adversely affect quality of life. Ionizing radiation has been shown to destroy immature primordial follicles and maturing secondary and antral follicles (1–3,12). In the latter follicles, apoptotic death of cells in the granulosa cell layers surrounding the oocyte appears to occur first, followed by death of the oocyte. COV434 granulosa cells are derived from a human granulosa cell tumour; however, they possess many properties of normal granulosa cells that make them useful as models for understanding mechanisms by which ionizing radiation destroys growing follicles (36,49).

GCL is a heterodimer composed of GCLC and GCLM. Although GCLC possesses the catalytic activity, GCLM decreases the K_m for glutamate and ATP and increases the K_i

for GSH, thereby greatly increasing the catalytic efficiency of the enzyme (25). In the present experiments, we generated stably transfected COV434 human granulosa tumour cell lines that constitutively overexpressed *Gclc*, *Gclm* or both *Gclc* and *Gclm*. Total intracellular GSH levels increased significantly by 1.5- to 2.2-fold, depending on the cell line, as a result of increased GCLC and/or GCLM protein levels and increased GCL catalytic activity. Several studies have shown that overexpression of *Gclc*, *Gclm* or both *Gclc* and *Gclm* results in increased GCL protein expression and enzymatic activity as well as in higher total GSH levels in other cell types (50–57). The effect of GCL overexpression often varied in an unpredictable manner between different stably transfected clones. Indeed, the same cell line transfected with the same amount of GCL overexpression vector can result in various clones that have differing degrees of GCL protein expression, enzymatic activity and/or total GSH levels (50,51,56). In some instances, overexpression of *Gclc* alone maximally increased total GSH levels; in others overexpression of *Gclm* alone had the greatest effect and in yet others co-transfection yielded the highest GSH levels (50,53,54,58). When various molar ratios of *Gclc* to *Gclm* cDNA ranging from 4:1 to 1:4 were used to co-transfect COS-7 cells, there were no significant differences in GSH concentration among the co-transfected cells regardless of the molar ratio used. In the same study, when COS-7 cells were transfected with *Gclc* only, the effect on GSH levels was not significantly different from the changes seen in the various co-transfected clones (53). These results suggest that the copy number of integrated transgenes has the greatest effect on total GSH levels and not the absolute amount of *Gclc* and/or *Gclm* cDNA that is introduced into the transfected cells. Because transgene integration is a random event, one cannot predict the results of single-gene or double-gene transfection on biochemical end points. When *Gclc* and/or *Gclm* are overexpressed to various randomly generated degrees, the bioavailability of the opposite heterodimer may become limiting. Similarly, the bioavailability of L-cysteine, the rate-limiting substrate in GSH synthesis, may become limiting (59). Finally, the effect of GCL overexpression on total GSH levels also seems to be highly cell type specific (56).

The results of the present studies add to the growing body of evidence that GSH is involved in protecting cells against ROS-mediated apoptosis. In particular, this and our previous studies support an anti-apoptotic role of GSH in granulosa cells. Induction of granulosa cell apoptosis by hormone withdrawal and by the polycyclic aromatic hydrocarbon dimethylbenz[*a*]anthracene was preceded by an early rise in ROS in cultured antral follicles (60,61). Similarly, induction of apoptosis by the anticancer drug cyclophosphamide in COV434 human granulosa cells was preceded by an early increase in ROS (35). The induction of apoptosis by all these stimuli was enhanced by GSH depletion and attenuated by supplementation of GSH (35,60,61). *Gclc* overexpression in transgenic flies increased resistance to H_2O_2 treatment and increased mean fly lifespan by inhibiting age-associated ROS accumulation that culminates in neuronal apoptosis (54). Similarly, *Gclc* overexpression rescued primary rat cortical neurons from undergoing apoptosis induced by exogenous nitrosative stress (58). Rat *Gclc* overexpression in Chinese hamster ovary cells enhanced resistance to cytotoxic effects of *tert*-butyl hydroperoxide treatment (51), and overexpression of both *Gclc* and *Gclm* cDNAs in Hepa-1 cells conferred a protective effect against H_2O_2-induced single-strand DNA breaks (55). In the present study, GCL

subunit-overexpressing cells were challenged with the pro-oxidant H_2O_2 and then assayed for cell viability. For all cell genotypes, granulosa cell viability decreased in a dose-dependent manner with H_2O_2 treatment; however, viability decreased significantly less in *Gclc*-transfected cells than in control cells, showing that these cells were better able to respond to the oxidative assault. These results support the hypothesis that GSH is involved in protecting granulosa cells against ROS-mediated cell death. It is important to note that in our experiments, the C6a cell line, which displayed the greatest increase in total GSH levels relative to parental controls, was most protected when challenged with H_2O_2. Three other GCL subunit-transfected cell lines, which had smaller increases in GSH concentrations relative to control cells, were also protected, but to a lesser extent than C6a cells. Moreover, the protective effect of stable transfection with *Gclc* in the C6a cell line was reversed by suppression of GSH synthesis with BSO, an inhibitor of GCL activity.

When we irradiated parental COV434 cells, we noted a dose-dependent increase in ROS generation within 30 min of irradiation that persisted at 2, 6, 24 and 48 h. GCL-over-expressing human granulosa cells also demonstrated rapid, dose-dependent increases in ROS generation after irradiation; however, radiation-induced ROS generation was significantly attenuated in cells overexpressing GCL. Cells that produced the highest levels of GSH (i.e. C6a) were most protected against radiation-induced ROS. Several studies have also demonstrated that ROS increase after radiation exposure in other cell types. Immediately after exposing U937 human premonocytic leukaemic lymphoma cells to 2 Gy of γ-irradiation, levels of intracellular ROS and specifically H_2O_2 increased 2-fold. This increase in ROS generation was accompanied by a smaller, but significant, increase in lipid peroxidation and protein oxidation (62). *In vivo* radiation exposure has also been shown to increase generation of hepatic nitrosative species after 24 h (33). Primary rat neural precursor cells exhibited a dose-dependent increase in ROS over the first 12 h after exposure to X-rays, with maximal ROS levels being attained at 12 h (45). Post-irradiation ROS levels remained persistently elevated over a 3- to 4-week interval and then returned to background levels (45). When exposed to 250 MeV protons, neural precursor cells exhibited significant and dose-dependent increases in ROS, with maximal ROS levels at 6 h (63). Different radiation sources and regimes and different cell types, therefore, seem to elicit distinct temporal changes in ROS generation. Moreover, when primary neural precursor cells were pretreated with the pro-oxidant H_2O_2, they became sensitized to both proton and γ-rays (64).

In the present studies, caspase 3 activation and DNA fragmentation measured by TUNEL were minimally increased at 2 h after irradiation and were prominently increased by 6 h in both parental and empty vector-transfected control cell lines. The *Gclc*-transfected cell line C6a was protected against radiation-induced apoptosis. It is well established that radiation induces acute apoptotic cell death in various cell types including primary neural precursor cells (45), U937 cells (62), mouse hepatic tissue (32) and rat hepatic tissue (33). Others have established that pharmacologic replenishment of GSH or other thiol-containing reducing agents can protect cells against radiation-induced apoptosis or cell death. The GSH precursor, NAC, dose-dependently attenuated hepatic toxicity induced by ionizing radiation, as assessed by increased DNA damage, lipid peroxidation and apoptosis in mice (32) and rats (33). In both instances, pretreatment with NAC was shown to

significantly and dose dependently increase GSH levels, suggesting that GSH, not NAC, mediates the protective effect against radiation-induced cell death. To our knowledge, the present study is the first to demonstrate a protective effect of genetic enhancement of GSH synthesis against radiation-induced cell death.

It is important to identify the key elements involved in follicular apoptosis in an effort to develop appropriate therapies for the protection and survival of these limited ovarian structures. We studied granulosa cells because it has been noted that follicular apoptosis often begins in the granulosa cells. Targeted GSH supplementation, for example using techniques such as biodegradable nanoparticle-controlled or magnetically controlled systems to deliver *Gclc* expression vectors to the ovary, could in the future serve as methods for protecting follicles in young women being treated with radiation therapy (65,66). Currently, the only methods for conserving these follicles are invasive and include ovarian transposition to reposition the ovaries outside of the irradiation field, sex hormone replacement or collection and cryopreservation of embryos, oocytes and ovarian tissue (1,2).

Along the same lines, it is imperative to understand the mechanisms by which cancerous cells circumvent the effects of conventional cancer treatments. Although COV434 cells have many characteristics of normal human granulosa cells and can serve as a model to understand normal granulosa cells (35,36), one cannot ignore the fact that they were derived from a granulosa cell tumour. These cells, therefore, inherently possess many characteristics of both primary granulosa cells and malignant cancerous cells. Our study demonstrates that increased GSH synthesis is radioprotective in tumour cells. Other researchers have shown that GSH depletion may serve as a potential therapy to radiosensitize tumour cells prior to the onset of radiotherapy (28–33).

Our studies suggest that polymorphisms of the *Gclc* and *Gclm* genes found in the human population may be responsible, at least in part, for interindividual variation in sensitivity to radiation-induced ovarian damage. In African American, Caucasian, Asian and Hispanic populations, the *Gclc* gene contains a GAG trinucleotide repeat in the 5′ untranslated region. There are five reported alleles with 4, 7, 8, 9 or 10 GAG repeats (67,68). The genetic polymorphisms that cause a deficit in *Gclc* expression, GCL activity and GSH biosynthesis have been associated with schizophrenia—a disease whose pathogenesis is associated with oxidative stress and GSH deficiency (69). There have also been two polymorphisms identified in an Asian population in the 5′-flanking region of the *Gclm* gene, each with two distinct allele variations. The −588T allele variant of the −588C/T polymorphism is positively correlated with decreased *Gclm* expression, decreased plasma GSH levels and increased risk of oxidative stress-induced vascular injury (70,71). By identifying correlations between allele frequencies and radiosensitivity, it may be possible to predict the probability of infertility resulting from radiotherapy.

In conclusion, we have shown that exposure of human granulosa cells to therapeutic doses of ionizing radiation rapidly increases intracellular ROS, followed by induction of apoptosis. Further, we have shown that granulosa cells with increased capacity to synthesize GSH, due to stable over-expression of GCL subunits, are protected against oxidant- and radiation-induced apoptosis. These results provide support for the hypothesis that the rise in ROS mediates the induction of

apoptosis in granulosa cells by ionizing radiation and contribute to our understanding of the effects of radiation on normal ovarian follicles as well as ovarian tumours.

References

1. Meirow, D. and Nugent, D. (2001) The effects of radiotherapy and chemotherapy on female reproduction. *Hum. Reprod. Update*, **7**, 535–543.
2. Lo Presti, A., Ruvulo, G., Gancitano, R. A. and Cittadini, E. (2004) Ovarian function following radiation and chemotherapy for cancer. *Eur. J. Obstet. Gynecol. Reprod. Biol.*, **113**, S33–S40.
3. Hanoux, V., Pairault, C., Bakalska, M., Habert, R. and Livera, G. (2007) Caspase-2 involvement during ionizing radiation-induced oocyte death in the mouse ovary. *Cell Death Differ.*, **14**, 671–681.
4. Lee, C. J. and Yoon, Y.-D. (2005) γ-Radiation-induced follicular degeneration in the prepubertal mouse ovary. *Mutat. Res.*, **578**, 247–255.
5. Wallace, W. H. B., Shalet, S. M., Hendry, J. H., Morris-Jone, P. H. and Gattamaneni, H. R. (1989) Ovarian failure following abdominal irradiation in childhood: the radiosensitivity of the human oocyte. *Br. J. Radiol.*, **62**, 995–998.
6. Wallace, W. H. B., Thomson, A. B. and Kelsey, T. W. (2003) The radiosensitivity of the human oocyte. *Hum. Reprod.*, **18**, 117–121.
7. Lee, C. J., Park, H. H., Do, B. R., Yoon, Y. D. and Kim, J. K. (2000) Natural and radiation-induced degeneration of the primordial and primary follicles in the mouse ovary. *Anim. Reprod. Sci.*, **59**, 109–117.
8. Byskov, A. G., Faddy, M. J., Lemmen, J. G. and Andersen, C. Y. (2005) Eggs forever? *Differentiation*, **73**, 438–446.
9. Kim, M.-R. and Tilly, J. L. (2004) Current concepts in Bcl-2 family member regulation of female germ cell development and survival. *Biochim. Biophys. Acta*, **1644**, 205–210.
10. Hirshfield, A. N. (1988) Size-frequency analysis of atresia in cycling rats. *Biol. Reprod.*, **38**, 1181–1188.
11. Tilly, J. L. and Robles, R. (1999) Apoptosis and its impact in clinical reproductive medicine. In Fauser, B. C. J. M., Rutherford, A. J., Strauss, J. F.III and Van Steirteghem, A. (eds), *Molecular Biology in Reproductive Medicine*. Parthenon, New York, NY, pp. 79–101.
12. Kim, J. K. and Lee, C. J. (2000) Effect of exogenous melatonin on the ovarian follicles in γ-irradiated mouse. *Mutat. Res.*, **449**, 33–39.
13. Morita, Y., Perez, G. I., Paris, F. *et al.* (2000) Oocyte apoptosis is suppressed by disruption of the acid sphingomyelinase gene or by sphingosine-1-phosphate therapy. *Nat. Med.*, **6**, 1109–1114.
14. Ward, J. F. (1988) DNA damage produced by ionizing radiation in mammalian cells: identities, mechanisms of formation, and reparability. *Prog. Nucleic Acid Res. Mol. Biol.*, **35**, 95–125.
15. Ward, J. F. (1994) The complexity of DNA damage: relevance to biological consequences. *Int. J. Radiat. Biol.*, **66**, 427–432.
16. Riley, P. A. (1994) Free radicals in biology: oxidative stress and the effects of ionizing radiation. *Int. J. Radiat. Biol.*, **65**, 27–33.
17. Wiseman, H. and Halliwell, B. (1996) Damage to DNA by reactive oxygen and nitrogen species: role in inflammatory disease and progression to cancer. *Biochem. J.*, **313**, 17–29.
18. Hornsby, P. J. and Crivello, J. F. (1983) The role of lipid peroxidation and biological antioxidants in the function of the adrenal cortex. Part I: a background review. *Mol. Cell. Endocrinol.*, **30**, 1–20.
19. Stadtman, E. R. and Oliver, C. N. (1991) Metal-catalyzed oxidation of proteins. *J. Biol. Chem.*, **266**, 2005–2008.
20. Dayal, D., Martin, S. M., Limoli, C. L. and Spitz, D. R. (2008) Hydrogen peroxide mediates the radiation-induced mutator phenotype in mammalian cells. *Biochem. J.*, **413**, 185–191.
21. Spitz, D. R., Azzam, E. I., Li, J. J. and Gius, D. (2004) Metabolic oxidation/reduction reactions and cellular response to ionizing radiation: a unifying concept in stress response biology. *Cancer Metastasis Rev.*, **23**, 311–322.
22. Griffith, O. W. and Mulcahy, R. T. (1999) The enzymes of glutathione synthesis: gamma-glutamylcysteine synthetase. *Adv. Enzymol. Relat. Areas Mol. Biol.*, **73**, 209–267.
23. Soltaninassab, S. R., Sekhar, K. R., Meredith, M. J. and Freeman, M. L. (2000) Multi-faceted regulation of γ-glutamylcysteine synthetase. *J. Cell. Physiol.*, **182**, 163–170.
24. Anderson, M. E. and Luo, J. L. (1998) Glutathione therapy: from prodrugs to genes. *Semin. Liver Dis.*, **18**, 415–424.
25. Chen, Y., Shertzer, H. G., Schneider, S. N., Nebert, D. W. and Dalton, T. P. (2005) Glutamate cysteine ligase catalysis. Dependence on ATP levels and modifier subunit for regulation of tissue glutathione levels. *J. Biol. Chem.*, **280**, 33766–33774.
26. Calvert, P., Yao, K. S., Hamilton, T. C. and O'Dwyer, P. J. (1998) Clinical studies of reversal of drug resistance based on glutathione. *Chem. Biol. Interact.*, **111–112**, 213–224.
27. Godwin, A. K., Meister, A., O'Dwyer, P. J., Huang, C.-S., Hamilton, T. C. and Anderson, M. E. (1992) High resistance to cisplatin in human ovarian cancer cell lines is associated with marked increase of glutathione synthesis. *Proc. Natl Acad. Sci. USA*, **89**, 3070–3074.
28. Estrela, J. M., Ortega, A. and Obrador, E. (2006) Glutathione in cancer biology and therapy. *CRC Crit. Rev. Clin. Lab. Sci.*, **43**, 143–181.
29. Clark, E. P. (1986) Thiol-induced biochemical modification of chemo- and radioresponses. *Int. J. Radiat. Oncol. Biol. Phys.*, **12**, 1121–1126.
30. Biaglow, J. E., Clark, E. P., Epp, E. R., Morse-Guadio, M. and Varnes, M. E. (1983) Non-protein thiols and the radiation response of A549 human lung carcinoma cells. *Int. J. Radiat. Biol.*, **44**, 489–495.
31. Biaglow, J. E., Varnes, M. E., Tuttle, S. W., Oleinick, N. L., Glazier, K., Clark, E. P., Epp, E. R. and Dethlefsen, L. A. (1986) The effect of L-buthionine sulfoximine on the aerobic radiation response of A549 human lung carcinoma cells. *Int. J. Radiat. Oncol. Biol. Phys.*, **12**, 1139–1142.
32. Liu, Y., hang, H., Zhang, L., Zhou, Q., Wang, X., Long, J., Dong, T. and Zhao, W. (2007) Antioxidant *N*-acetylcysteine attenuates the acute liver injury caused by X-ray in mice. *Eur. J. Pharmacol.*, **575**, 142–148.
33. Mansour, H. H., Hafez, H. F., Fahmy, N. M. and Hanafi, N. (2008) Protective effect of *N*-acetylcysteine against radiation induced DNA damage and hepatic toxicity in rats. *Biochem. Pharmacol.*, **75**, 773–780.
34. van den Berg-Bakker, C. A. M., Hegemeijer, A., Franken-Meijer, A., Franken-Postma, E. M., Smit, V. T. H. B.M., Kuppen, P. J. K., Ravenswaay-Claasen, H. H., Cornelisse, C. J. and Schrier, P. I. (1993) Establishment and characterization of 7 ovarian carcinoma cell lines and one granulosa tumor cell line: growth features and cytogenetics. *Int. J. Cancer*, **53**, 613–620.
35. Tsai-Turton, M., Luong, B. T., Tan, Y. and Luderer, U. (2007) Cyclophosphamide-induced apoptosis in COV434 human granulosa cells involves oxidative stress and glutathione depletion. *Toxicol. Sci.*, **98**, 216–230.
36. Zhang, H., Vollmer, M., De Geyter, M. *et al.* (2000) Characterization of an immortalized human granulosa cell line (COV434). *Mol. Hum. Reprod.*, **6**, 146–153.
37. Kang, Y., Qiao, X., Jurma, O., Knusel, B. and Andersen, J. K. (1997) Cloning/brain localization of mouse glutamylcysteine synthetase heavy chain mRNA. *Neuroreport*, **8**, 2053–2060.
38. Reid, L. L., Botta, D., Shao, J., Hudson, F. N. and Kavanagh, T. J. (1997) Molecular cloning and sequencing of the cDNA encoding mouse glutamate-cysteine ligase regulatory subunit. *Biochim. Biophys. Acta*, **1353**, 107–110.
39. Griffith, O. W. (1980) Determination of glutathione and glutathione disulfide using glutathione reductase and 2-vinylpyridine. *Anal. Biochem.*, **106**, 207–212.
40. Tsai-Turton, M. and Luderer, U. (2005) Gonadotropin regulation of glutamate cysteine ligase catalytic and modifier subunit expression in the rat ovary is subunit and follicle stage-specific. *Am. J. Physiol.*, **289**, E391–E402.

41. Thompson, S. A., White, C. C., Krejsa, C. M., Diaz, D., Woods, J. S., Eaton, D. L. and Kavanagh, T. J. (1999) Induction of glutamate-cysteine ligase (γ-glutamylcysteine synthetase) in the brains of adult female mice subchronically exposed to methylmercury. *Toxicol. Lett.*, **110**, 1–9.

42. White, C. C., Viernes, H., Kresja, C. M., Botta, D. and Kavanagh, T. J. (2003) Fluorescence-based microtiter plate assay for glutamate-cysteine ligase activity. *Anal. Biochem.*, **318**, 175–180.

43. LeBel, C. P., Ishiropoulos, H. and Bondy, S. C. (1992) Evaluation of the probe 2′,7′-dichlorofluorescin as an indicator of reactive oxygen species formation and oxidative stress. *Chem. Res. Toxicol.*, **5**, 227–231.

44. Wardman, P. (2007) Fluorescent and luminescent probes for measurement of oxidative and nitrosative species in cells and tissues: progress, pitfalls, and prospects. *Free Radic. Biol. Med.*, **43**, 995–1022.

45. Limoli, C. L., Giedzinski, E., Rola, R., Otsuka, S., Palmer, T. D. and Fike, J. R. (2004) Radiation response of neural precursor cells: linking cellular sensitivity to cell cycle checkpoints, apoptosis, and oxidative stress. *Radiat. Res.*, **161**, 17–27.

46. Wang, H. and Joseph, J. A. (1999) Quantifying cellular oxidative stress by dichlorofluorescein assay using microplate reader. *Free Radic. Biol. Med.*, **27**, 612–616.

47. Luderer, U., Diaz, D., Faustman, E. M. and Kavanagh, T. J. (2003) Localization of glutamate cysteine ligase subunit mRNA within the rat ovary and relationship to follicular atresia. *Mol. Reprod. Dev.*, **65**, 254–261.

48. Pasternack, B. S. and Shore, R. E. (1982) Analysis of dichotomous response data from toxicological experiments involving stable laboratory mouse populations. *Biometrics*, **38**, 1057–1067.

49. Havelock, J. C., Rainey, W. E. and Carr, B. R. (2004) Ovarian granulosa cell lines. *Mol. Cell. Endocrinol.*, **228**, 67–78.

50. Botta, D., Franklin, C. C., White, C. C., Kresja, C. M., Dabrowski, M. J., Pierce, R. H., Fausto, N. and Kavanagh, T. J. (2004) Glutamate-cysteine ligase attenuates TNF-induced mitochondrial injury and apoptosis. *Free Radic. Biol. Med.*, **37**, 632–642.

51. Fernandes, C. J., Rong, L., Tamura, T., Stewart, K. D., Rogers, L. K., McMicken, H. W., Elliston, J. F., Hansen, T. N. and Smith, C. V. (2002) Stable transfection of Chinese hamster ovary cells with glutamate-cysteine ligase catalytic subunit cDNA confers increased resistance to tert-butyl hydroperoxide toxicity. *Toxicol. Lett.*, **136**, 107–120.

52. Manna, S. K., Kuo, M. T. and Aggarwal, B. B. (1999) Overexpression of γ-glutamylcysteine synthetase suppresses tumor necrosis factor-induced apoptosis and activation of nuclear transcription factor-kappa B and activator protein-1. *Oncogene*, **18**, 4371–4382.

53. Mulcahy, R. T., Bailey, H. H. and Gipp, J. J. (1995) Transfection of complementary cDNAs for the heavy and light subunits of γ-glutamylcysteine synthetase results in an elevation of intracellular glutathione and resistance to melphalan. *Cancer Res.*, **55**, 4771–4775.

54. Orr, W. C., Radyuk, S. N., Prabhudesai, L., Toroser, D., Benes, J. J., Luchak, J. M., Mockett, R. J., Rebrin, I., Hubbard, J. G. and Sohal, R. S. (2005) Overexpression of glutamate-cysteine ligase extends life span in *Drosophila melanogaster*. *J. Biol. Chem.*, **280**, 37331–37338.

55. Shi, S., Hudson, F. N., Botta, D., McGrath, M. B., White, C. C., Neff-Laford, H. D., Dabrowski, M. J., SIngh, N. P. and Kavanagh, T. J. (2007) Over expression of glutamate cysteine ligase increases cellular resistance to H_2O_2-induced DNA single-strand breaks. *Cytometry Part A*, **71A**, 686–692.

56. Tipnis, S. R., Blake, D. G., Sheperd, A. G. and McLellan, L. I. (1999) Overexpression of the regulatory subunit of γ-glutamylcysteine synthetase in HeLa cells increases γ-glutamylcysteine synthetase activity and confers drug resistance. *Biochem. J.*, **337**, 559–566.

57. Tran, P. O. T., Parker, S. M., LeRoy, E., Franklin, C. C., Kavanagh, T. J., Zhang, T., Zhou, H., Vliet, P., Oseid, E., Harmon, J. S. and Robertson, R. P. (2004) Adenoviral overexpression of the glutamylcysteine ligase catalytic subunit protects pancreatic islets against oxidative stress. *J. Biol. Chem.*, **279**, 53988–53993.

58. Diaz-Hernandez, J. I., Almeida, A., Delgado-Esteban, M., Fernandez, E. and Bolanos, J. P. (2005) Knockdown of glutamate-cysteine ligase by small hairpin RNA reveals that both catalytic and modulatory subunits are essential for the survival of primary neurons. *J. Biol. Chem.*, **280**, 38992–39001.

59. Griffith, O. W. (1999) Biologic and pharmacologic regulation of mammalian glutathione synthesis. *Free Radic. Biol. Med.*, **27**, 922–935.

60. Tsai-Turton, M. and Luderer, U. (2006) Opposing effects of glutathione depletion and FSH on reactive oxygen species and apoptosis in cultured preovulatory rat follicles. *Endocrinology*, **147**, 1224–1236.

61. Tsai-Turton, M., Nakamura, B. N. and Luderer, U. (2007) Induction of apoptosis by 9,10-dimethyl-1,2-benzanthracene (DMBA) in cultured preovulatory rat follicles is preceded by a rise in reactive oxygen species and is prevented by glutathione. *Biol. Reprod.*, **77**, 442–451.

62. Lee, J. H., Tak, J. K., Park, K. M. and Park, J.-W. (2007) N-t-butyl hydroxylamine regulates ionizing radiation-induced apoptosis in U937 cells. *Biochimie*, **89**, 1509–1516.

63. Giedzinski, E., Rola, R., Fike, J. R. and Limoli, C. L. (2005) Efficient production of ROS in neural precursor cells after exposure to 250 MeV protons. *Radiat. Res.*, **164**, 540–544.

64. Limoli, C. L., Giedzinski, E., Baure, J., Rola, R. and Fike, J. R. (2006) Altered growth and radiosensitivity in neural precursor cells subjected to oxidative stress. *Int. J. Radiat. Biol.*, **82**, 640–647.

65. Panyam, J. and Labhasetwar, V. (2003) Biodegradable nanoparticles for drug and gene delivery to cells and tissue. *Adv. Drug Deliv. Rev.*, **55**, 329–347.

66. Lübbe, A. S., Alexiou, C. and Bergemann, C. (2001) Clinical applications of magnetic drug targeting. *J. Surg. Res.*, **95**, 200–206.

67. Walsh, A. C., Feulner, J. A. and Reilly, A. (2001) Evidence for functionally significant polymorphism of human glutamate cysteine ligase catalytic subunit: association with glutathione levels and drug resistance in the National Cancer Institute tumor cell line panel. *Toxicol. Sci.*, **61**, 218–223.

68. Walsh, A. C., Li, W., Rosen, D. R. and Lawrence, D. A. (1996) Genetic mapping of GLCLC, the human gene encoding the catalytic subunit of gamma-glutamyl-cysteine synthetase, to chromosome band 6p12 and characterization of a polymorphic trinucleotide repeat within its 5′ untranslated region. *Cytogenet. Cell Genet.*, **75**, 14–16.

69. Gysin, R., Kraftsik, R., Sandell, J. *et al.* (2007) Impaired glutathione synthesis in schizophrenia: convergent genetic and functional evidence. *Proc. Natl Acad. Sci. USA*, **104**, 16621–16626.

70. Nakamura, S.-I., Kugiyama, K., Sugiyama, S., Miyamoto, S., Koide, S.-I., Fukushima, H., Honda, O., Yoshimura, M. and Ogawa, H. (2002) Polymorphism in the 5′-flanking region of the human glutamate-cysteine ligase modifier subunit gene is associated with myocardial infarction. *Circulation*, **105**, 2968–2973.

71. Nakamura, S.-I., Sugiyama, S., Fujioka, D., Kawabata, K.-I., Ogawa, H. and Kugiyama, K. (2003) Polymorphism in glutamate cysteine ligase modifier subunit gene is associated with impairment of nitric oxide-mediated coronary vasomotor dilation. *Circulation*, **108**, 1425–1427.